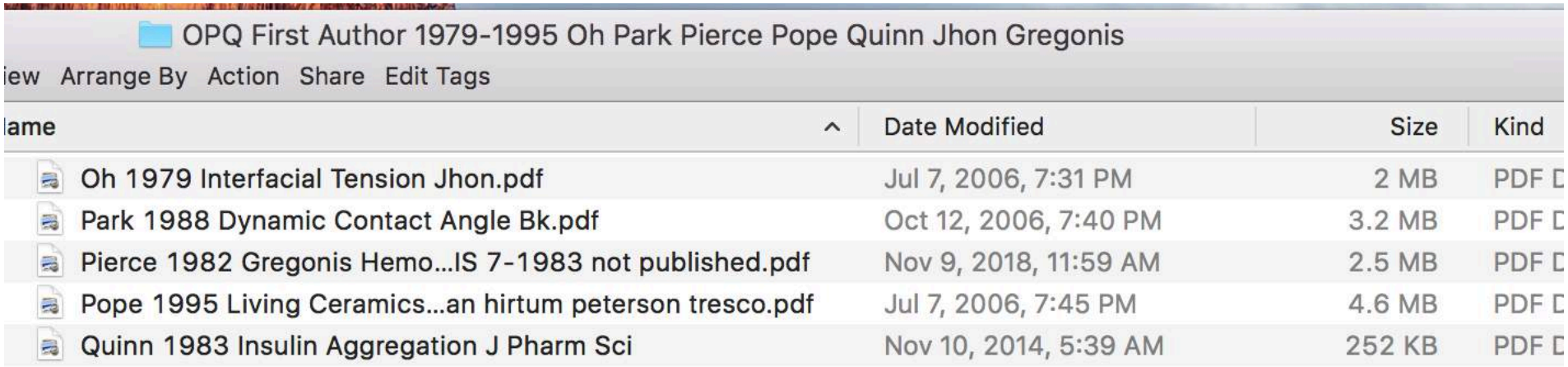
OPQ First Author 1979-1995 Oh Park Pierce Pope Quinn Jhon Gregonis
iew Arrange By Action Share Edit Tags
lame
Date Modified
Size
Kind
Oh 1979 Interfacial Tension Jhon.pdf
Jul 7, 2006, 7:31 PM
2 MB
PDF D
Park 1988 Dynamic Contact Angle Bk.pdf
Oct 12, 2006, 7:40 PM
3.2 MB
PDF D
Pierce 1982 Gregonis Hemo...IS 7-1983 not published.pdf
Nov 9, 2018, 11:59 AM
2.5 MB
PDF D
Pope 1995 Living Ceramics...an hirtum peterson tresco.pdf
Jul 7, 2006, 7:45 PM
4.6 MB
PDF D
Quinn 1983 Insulin Aggregation J Pharm Sci
Nov 10, 2014, 5:39 AM
252 KB
PDF D

OH-1

DAEHAN HWAHAK HWOEJEE
(*Journal of the Korean Chemical Society*)
Vol. 23, No. 4, 1979
Printed in the Republic of Korea

용융 고분자간의 계면장력에 대한 이론적 예측

吳英基 · Joseph D. Andrade* · 全武植

한국과학원 화학과

(1979. 5. 1 접수)

Theoretical Estimation of Interfacial Tension between Molten Polymers

Youngie Oh, Joseph D. Andrade* and **Mu Shik Jhon**

Department of Chemistry, Korea Advanced Institute of Science, Seoul, Korea

(Received May 1, 1979)

요 약. 특성구조액체이론(significant structure theory of liquids)에 입각하여, 섞이지 않는 두 용융 고분자중에서의 계면장력을 예측하는 간단한 계산방법을 연구하였다. 접착에너지는 응집에너지들의 기하평균과 보정항의 곱으로 표시되며, 응집에너지는 고분자 사슬의 격자상을 가정하므로써 계산된다. 계면장력을 계산함에 있어서 고분자사슬의 구성요소간 분산력(dispersion force) 외에 극성력(polar force)를 포함시켜야 함이 확인되었다.

. ABSTNACT. A simple method to calculate the interfacial tension between two immiscible molten polymers has been developed. The theory is based on the significant structure theory of liquids. The energy of adhesion is expressed as a geometric mean of the cohesion energies multiplied by correction factor (Φ_{12}), $\Delta E_{12}=\Phi_{12}\sqrt{\Delta E_{11}\Delta E_{22}}$. In the calculation of ΔE_{11} and ΔE_{22}, a quasilattice of polymer chains has been assumed. It is assured that, besides the dispersion force, the polar force interactions between polymer constituent groups should be considered in the calculation of the interfacial tensions.

INTRODUCTION

Knowledge of surface and interfacial tension can provide informations on the intermolecular forces and structural characterestics of condensed matters. The surface tension of molten polymers against air has been a subject of both experimental and theoretical studies[1~8], and the interfacial tension between two immiscible molten polymers has been measured for various polymeric materials[8~10]. We have, recently, examined the surface tension of amorphous polymers based on the significant structure theory of liquids[11]. Using the same framework, we now evaluate the interfacial tension between two molten polymers.

Since the interfacial tension is the difference between the free energy of the interfacial layer and that of the bulk, both the energy and entropy terms must be considered if one is to obtain a complete picture of the interfacial region. The energy term is attributed to the

* University of Utah, Salt Lake City, Utah 84112, U.S.A.

fact that a molecule (or chain constituent group) experiences a modified configurational energy due to the replacement of some fraction of its near neighbors by different molecular species at the interface. And also, a molecule (or the chain constituent group) at the interface occupies a modified free volume due to the replaced constraining neighbors, thus the entropy term may arise.

In the calculation of the interfacial tension for molten polymers, the two main assumptions are employed:

(i) the boundary between two phases is sharp, and the two different flat monomolecular layers at the boundary only contribute to the interfacial tension;

(ii) the free volume of a chain constituent group in the boundary layer is equal to the one in the interior.

Assumption (i) is based on the analogy of the monolayer approximation in calculation of surface tension for simple liquids[22]. For the liquid-air interfacial system (*i.e.*, the liquid surface), surface molecules (or chain constituent groups) experience enhanced freedom of movements due to the loss of some fraction of constraining nearest neighbors.[11] For the molecules at the liquid-liquid interface, the freedom of movements is not enhanced so much as the surface molecules due to the new constraining neighbors in one direction, thus the assumption (ii) is introduced.

Ignoring the entropy effect according to the assumption (ii), the interfacial tension γ_{12} is expressed in terms of the energy of adhesion per unit area for the interface between the phases 1 and 2, ΔE_{12}, and the energy of cohesion per unit area for each phases, ΔE_{11} and ΔE_{22},

$$\gamma_{12}=\frac{\Delta E_{11}}{2}+\frac{\Delta E_{22}}{2}-\Delta E_{12} \tag{1}$$

A diagram of the process for thermodynamic definition of ΔE_{11}, ΔE_{22}, and ΔE_{12} are illustrated in *Fig.* 1. It has been recognized by Girifalco and Good[12] that the energy of adhesion is given by the geometric mean of the energy of cohesion multiplied by a correction factor Φ_{12},

$$\Delta E_{12}=\Phi_{12}(\Delta E_{11}\Delta E_{22})^{1/2} \tag{2}$$

And they derived the expression for Φ_{12} using a quasi-continuum model of condensed phase,

$$\Phi_{12}=\frac{A_{12}}{(A_{11}A_{22})^{1/2}}\ \frac{d_{11}d_{22}}{d_{12}^{2}} \tag{3}$$

Here, A_{11} and A_{22} are the inverse sixth power dispersion coefficients for molecular species 1 and 2 respectively, A_{12} is the dispersion coefficient for the interaction of molecular species 1 and 2; d_{11}, d_{22}, and d_{12} are the equilibrium separation distances between the two semi-infinite bodies of individual phases respectively. The problem is, then, reduced to the calculation of ΔE_{11} and ΔE_{22} for the molten polymeric systems through an appropriate model.

THEORY

The significant structure theory of liquids[13,14] has been widely applied. In this theory, the liquid is regarded as having a quasi-lattice structure in which the sites are occupied by

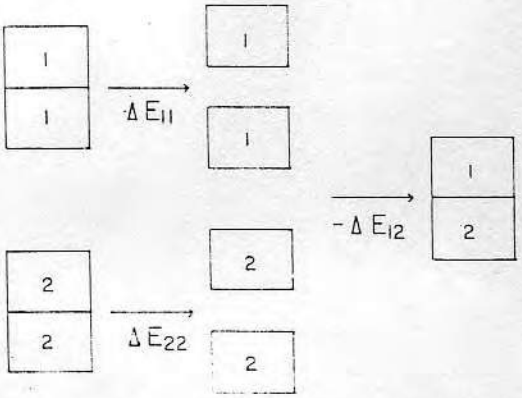

Fig. 1. A diagrammatic definition of energy of cohesion and adhesion.

molecules or by fluidized vacancies. Because these fluidized vacancies are moved about cooperatively by neighboring molecules jumping into them, a vacancy confers gas-like degrees of freedom on three vibrational degrees of freedom. If V is the molar volume of the fluid system and V_s measures molar volume occupied by molecules, then a vibrating molecule moves into a vacancy on $\frac{V-V_s}{V}$ of its excursions, conferring gas-like properties on this fraction of the degrees of freedom. Thus, a mole of liquid behaves as though it were made up of $N\frac{V-V_s}{V}$ gas molecules and $N\frac{V_s}{V}$ solid-like. Let us consider a surface of the liquid, whose area is Ω. If the surface is composed of M lattice sites, $M\frac{V_s}{V}$ sites are occupied by molecules and the remaining sites are occupied by fluidized vacancies. Since the fluidized vacancies confer gas-like properties on the neighboring moles, $M\frac{V_s}{V}$ molecules in the surface behave as though they were made up of $M\frac{V_s}{V}\ \frac{V-V_s}{V}$ gas molecules and $M\frac{V_s}{V}\ \frac{V_s}{V}$ solid-like. Per unit area of the surface, there are $\frac{1}{w}\ \frac{V_s}{V}\ \frac{V-V_s}{V}$ molecules of gas-like, and $\frac{1}{w}\left(\frac{V_s}{V}\right)^2$ molecules of solid-like, where $w\left(=\frac{\Omega}{M}\right)$ is the area occupied by a molecule.

In order to apply the model of significant liquid structures to the polymeric systems, we regard a chain molecule as being built up of identical repeating constituent groups neglecting end group effect. The size of a repeating constituent group is taken as a principal structural unit (*i.e.*, monomer unit), and assumed to be a mass point. Each repeating constituent group contributes to the lattice modes with its one-dimensional degree of freedom independently and contributes to the internal vibrations (*i.e.*, stretching and bending modes of the chain skeleton) with its remaining two dimensional degrees of freedom[15]. Therefore, the fluidized vacancies confer one dimensional gas-like degree of freedom on the neighboring chain constituent group.

Assuming that the gas-like properties of chain constituent group in the surface (or the interface) are not different from that in the bulk, the number of repeating constituent group in the surface, which are practically important to the interfacial tension, is then $\frac{1}{w}\left(\frac{V_s}{V}\right)^2$ where w is the area occupied by one monomer unit at the surface. Thus, the energy of cohesion can be expressed as

$$\Delta E_{11}=\frac{1}{w_1}\left(\frac{V_{s1}}{V_1}\right)^2[\phi_1'-\phi_1] \tag{4a}$$

$$\Delta E_{22}=\frac{1}{w_2}\left(\frac{V_{s2}}{V_2}\right)^2[\phi_2'-\phi_2] \tag{4b}$$

Here, ϕ_i' and ϕ_i represents the configurational energy of a constituent group in the surface and in the bulk respectively, the subscripts 1 and 2 denotes the different polymer species.

CALCULATION

The experiments of neutron scattering[16] and light scattering[17] from amorphous polymers have shown the persistence length (10~15Å) of chain segments and the existence of short range correlations due to packing of chain molecules, although no evidence of long range orientational order has been found. But the equilibrium properties of a condensed amorphous system depend inherently on the interaction energy between the objects which constitute the system. Since the interaction diminishes rapidly as the objects are distant apart from each other, one should consider a short range structure of the

gree of freedom
s to the internal
nd bending modes
its remaining two
on[15]. Therefore,
one dimensional
the neighboring

roperties of chain
(or the interface)
the bulk, the
nt group in the
important to the
$\left(\frac{V_s}{V}\right)^2$ where w
nomer unit at
of cohesion can

(4a)

(4b)

configurational
the surface
subscripts 1
ner species.

ttering[16] and
polymers have
10~15Å) of
of short range
in molecules,
orientational
equilibrium
hous system
tion energy
the system.
pidly as the
other, one
ture of the
ical Society

objects to evaluate to interaction energy. Thus, a lattice arrangement of solid-like chain constituent group, which follow a parallel alignment in the bulk and surface state, can be assumed (see *Fig.* 2.). From the assumed lattice model, and assuming the Lennard-Jones (6~12) potential, we have obtained the followings[11],

$$V_{si}=N\sigma_{0i}a_i^2 \tag{5a}$$

$$w_i=\sigma_{0i}a_i \tag{5b}$$

$$\psi_i=4\varepsilon_i\left(\frac{a_i}{\sigma_{0i}}\right)\left[3.1633\left(\frac{\sigma_i}{a_i}\right)^{12}-5.8869\left(\frac{\sigma_i}{a_i}\right)^{6}\right] \tag{5c}$$

$$\psi_i'=4\varepsilon_i\left(\frac{a_i}{\sigma_{0i}}\right)\left[2.3552\left(\frac{\sigma_i}{a_i}\right)^{12}-4.2201\left(\frac{\sigma_i}{a_i}\right)^{6}\right] \tag{5d}$$

where a_1 : the nearest neighboring distance between the polymer chain, σ_{0i} : distance between the neighboring monomer units in the same chain, ε_1 and σ_1 : Lennard-Jones(6~12) potential parameters.

Hence, by substituting the Eqs. (5a), (5b), (5c), and (5d) into the Eqs. (4a) and (4b) the energy of cohesion is written immediately as

$$\Delta E_{11}=\beta_1^{-3/2}\frac{\sigma_1^4}{(V_1/N)^2}\varepsilon_1[7.1072\beta_1^{5/2}-3.2324\beta_1^{11/2}] \tag{6a}$$

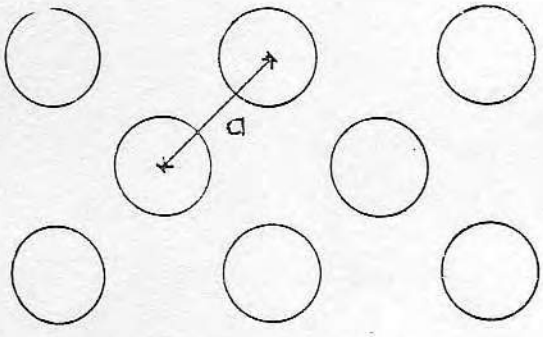

Fig. 2. A lattice arrangement of solid-like polymer chains.

$$\Delta E_{22}=\beta_2^{-3/2}\frac{\sigma_2^4}{(V_2/N)^2}\varepsilon_2[7.1072\beta_2^{5/2}-3.2324\beta_2^{11/2}] \tag{6b}$$

where

$$\beta_i=\frac{N\sigma_{0i}\sigma_i^2}{V_{si}}$$

The dimensionless parameter, β_i, has the same meaning of the Askadskii's packing coefficient[18] of the solid-like. The value $\beta_i=0.98$ best fits the experimental surface tensions of various molten polymers over a wide range of temperature[11].

An approximate method of estimating the (6~12) potential parameters, $\frac{\varepsilon}{k}$ and σ, for polymer constituent groups has been proposed by Davis[5]. His empirical formulas correlate the $\frac{\varepsilon}{k}$ and σ with the polarizability α and dia magnetic susceptbility χ as follows:

$$\ln(\sigma^2-5.4)=1.456+0.797\ln(\alpha\times10^{24}) \tag{7a}$$

$$\ln\left(\frac{\varepsilon}{k}\frac{\sigma^6}{10^4}\right)=-0.1445+1.1148\ln(-\alpha\chi\times10^{30}) \tag{7b}$$

The polarizabilities and diamagnetic susceptibilites are obtainable by adding atomic or partial group contributions from tables given by Van Krevelen[19]. In *Table* 1, the group values of α, χ, $\frac{\varepsilon}{k}$, and σ are summarized.

On the basis of the functional dependence of Eq. (7b) and the Kirkwood-Müller eqation, the expression for Φ_{12}, also, is proposed by Davis[5], *i. e.*,

$$\Phi_{12}=\frac{d_{11}d_{22}}{d_{12}^2}\left[\frac{2(\alpha_1\chi_1\alpha_2\chi_2)^{1/2}}{(\alpha_1\chi_2+\alpha_2\chi_1)}\right] \tag{8}$$

For the equilibrium d_{11}, d_{22}, and d_{12}, we assume the followings;

$$d_{12}=C\frac{d_{11}+d_{22}}{2} \tag{9a}$$

$$\frac{d_{11}}{d_{22}}=\frac{\sigma_1}{\sigma_2} \tag{9b}$$

where C is a proportional constant. At first sight, one might expect the value of C to be unity, however, the incompatibility of the two chemically dissimilar polymers suggests that the proportional constant must be somewhat larger than unity. The Eq. (8) is, rereduced to

$$\Phi_{12}=\left(\frac{1}{C}\right)^2\frac{4\sigma_1\sigma_2}{(\sigma_1+\sigma_2)^2}\left[\frac{2(\alpha_1\chi_1\alpha_2\chi_2)^{1/2}}{(\alpha_1\chi_1+\alpha_2\chi_1)}\right]^{1.1148} \tag{10}$$

With the aids of Eqs. (1), (2), (6a), (6b), (10), aad the value $\beta_i=0.98$, the equation for interfacial tension is rewritten as

$$\gamma_{12}=1.995\left\{\frac{\sigma_1^4}{2V_1^2}\left(\frac{\varepsilon_1}{k}\right)+\frac{\sigma_2^4}{2V_2^2}\left(\frac{\varepsilon_2}{k}\right)-\left(\frac{1}{C}\right)^2\right.$$
$$\frac{4\sigma_1\sigma_2}{(\sigma_1+\sigma_2)^2}\left[\frac{2(\alpha_1\chi_1\alpha_2\chi_2)^{1/2}}{\alpha_1\chi_2+\alpha_2\chi_1}\right]^{1.1148}$$
$$\left.\times\frac{\sigma_1^2\sigma_2^2}{V_1V_2}\left(\frac{\varepsilon_1}{k}\right)^{1/2}(\varepsilon_2/k)^{1/2}\right\} \tag{11}$$

Here, σ_i's in Angstroms, and V_i's are in cm²/mole. Calculations are carried out for 19-pairs of molten polymers in order to get the optimum value of the parameter C. When the value $\left(\frac{1}{C}\right)^2=0.96$ is taken, the Eq. (11) predicts the interfacial tensions at 150 °C within ±2.9 dyne/cm. In the calculations the observed molar volumes of molten polymers, which are shown in *Table* 1, are used. The results are given in *Table* 2.

Obviously, we have considered only dispersion interactions for the polymers whose constituent groups have permanent dipole moments. A rigorous treatment of the polar interaction in the polymeric system is quite difficult due to the complexity of the restricting force on the dipolar rotations. Neverthless, one can consider the simplified treatment of the polar force contributions to the interfacial tension assuming a free rotation of dipoles. In the case of freely rotating dipoles, any fixed orientation of the dipole persists for a very short period of time,

Table 1. Constituent group values for polarizabilities, molar diamagnetic susceptibilities, (6~12) potential parameters, dipole moments, and molar volumes at 150 °C.

Polymer constituents segments	$\alpha\cdot10^{24}$ (cc)	$-\chi\cdot10^{5}$ (cgs)	σ (Å)	ε/k (°K)	μ^a (Debyes)	V^b (cm³/mole)
$-CH_2-CH_2-$	3.68	22.8	4.19	225	0	36.1
$-CH(CH_3)-CH_2-$	5.49	34.1	4.70	275	0	54.0
$-C(CH_3)_2-CH_2-$	7.32	45.4	5.13	306	0	66.3
$-CH(C_6H_5)-CH_2-$	13.4	75.9	6.27	321	0.59	104.9
$-CH(OCCH_3)-CH_2-$ (O ‖)	8.01	48.5	5.29	308	1.78	79.4
$-C(COCH_3)-CH_2-$ (O ‖, CH_3 |)	9.81	58.5	5.65	317	1.60	88.5
$-C(COC_4H_7)-CH_2-$ (O ‖, CH_3 |)	15.3	92.6	6.57	351	1.57	145.9
$-CH_3-CH_2-O-$	4.34	27.3	4.38	251	1.30	42.8
$-Si(CH_3)_2-O-$	7.39	47.0	5.15	316	0.24	85.4

[a]Referencce (21); [b]References (6), (8) and (9).

Table 2. Comparison of calculated interfacial tension with experimental values.

Polymer pairs	γ_{12}(dyne/cm) at 150 °C		
	Calc. (I)	Calc. (II)[b]	Exp.[c]
Poly(ethylene) *vs.*			
Poly(propylene)	4.5	3.5	1.1
Poly(styrene)	8.1	7.1	5.7
Poly(vinyl acetate)	6.0	7.2	9.8
Poly(methyl methacrylate)	6.5	6.5	9.5
Poly(*n*-butyl methacrylate)	10.1	9.6	5.2
Poly(ethylene oxide)	4.2	6.1	5.4
Poly(dimethyl siloxane)	7.2	6.7	5.4
Poly(propylene) *vs.*			
Poly(styrene)	5.5	4.6	5.1
Poly(dimethyl siloxane)	4.7	4.3	3.0
Poly(isobutylene) *vs.*			
Poly(vinyl acetate)	4.0	5.2	7.4
Poly(dimethyl siloxane)	5.1	4.7	4.3
Poly(styrene) *vs.*			
Poly(vinyl acetate)	4.2	5.2	3.7
Poly(methyl methacrylate)	3.8	3.7	1.6
Poly(dimethyl siloxane)	5.2	4.7	6.0
Poly(vinyl acetate) *vs.*			
Poly(*n*-butyl methacrylate)	3.9	4.2	2.8
Poly(dimethyl siloxane)	3.2	3.3	7.4
Poly(methyl methacrylate) *vs.*			
Poly(*n*-butyl methacrylate)	4.0	3.6	1.8
Poly(ethylene oxide) *vs.*			
Poly(dimethyl siloxane)	6.1	6.6	9.8
Poly(dimethyl siloxane) *vs.*			
Poly(*n*-butyl methacrylate)	3.3	2.8	3.8

[a]Calculated from Eq. (11); [b]Calculated from Eq. (13); [c]References (8), (9) and (10).

and the average interaction energy between two dipoles is[20]

$$\varphi_{12}^{(p)} = -\frac{2\mu_1^2\mu_2^2}{3kTr_{12}^6} \tag{12}$$

with conventional notations. Inclusion of this term of dipolar interaction to the Lennard-Jones (6~12) potential energy expression results the following interfacial tension equation with the same procedure described in the ref. (11) and preceding section.

$$\gamma_{12} = 1.995\left\{\frac{\sigma_1^4}{2V_1^2}\left(\frac{\varepsilon_1}{k}+1.53\times10^7\frac{\mu_1^4}{\sigma_1^6T}\right)+\frac{\sigma_2^4}{2V_2^2}\left(\frac{\varepsilon_2}{k}+1.53\times10^7\frac{\mu_2^4}{\sigma_2^6T}\right)-\left(\frac{1}{C}\right)^2\frac{4\sigma_1\sigma_2}{(\sigma_1+\sigma_2)^2}\frac{\sigma_1^2\sigma_2^2}{V_1V_2}\left[\left(\frac{\varepsilon_1}{k}\right)^{1/2}\left(\frac{\varepsilon_2}{k}\right)^{1/2}\left(\frac{2(\alpha_1\chi_1\alpha_2\chi_2)^{1/2}}{\alpha_1\chi_2+\alpha_2\chi_1}\right)^{1.1148}+1.53\times10^7\frac{\mu_1^2\mu_2^2}{\sigma_1^3\sigma_2^3T}\right]\right\} \tag{13}$$

Here, σ_i's are in Angstoms, μ_i's are in Debyes, V_i's are in cm^3/mole, and T is the absolute temperature. The paramete C is readjusted, and the value $\left(\frac{1}{C}\right)^2=0.97$ predicts the interfacial tension at 150 °C within ±2.3 dyne/cm. The dipole moments of chain constituent groups are taken as the values of gaseous monomer molecules, and are shown in *Table* 1. The results are given in *Table* 2, and are compared with the experimental values.

DISCUSSION

The present work provides a semi-qualitative method for predicting the interfacial tension between two different polymer liquids. The model of significant liquid structures is employed to formulate the interfacial tension-equation. If the additional polar force interactions besides the dispersion-force interactions are included, better agreements between the calculated and observed values are achieved as shown in *Table* 2. This fact implies that the polar force interactions should be considered in the calculations of interfacial tensions for the polymers having permanent dipole moments in their constituent group, as well as the dispersion force interaction.

It may seems surprising that the values of ε/k and σ evaluated by a very crude method, and the assumption of freely rotating dipoles predict the interfacial tensions so well. In the

case where the hydrogen bonding occurs, the term which represents the hydrogen bonding effect is to be added.

ACKNOWLEDGEMENT

One of the authors (M. S. Jhon) express appreciation to Korea Science and Engineering Foundation for the financial support to continue U. S-Korea Cooperative Research.

REFERENCES

1. R. J. Roe, *Proc. Natl. Acd. Sci.* (*U.S.*), **56**, 819 (1966).
2. T. Nose, *Polymer J.*, **3**, 1 (1972).
3. C. W. Stewart and C. A. von Frankenberg, *J. Polymer Sci.*, A-2, **6**, 1686 (1968).
4. H. W. Kammer, *Z. Phys. Chemie, Leipzig*, **258**, 1149 (1977).
5. B. W. Davis, *J. Colloid Interface Sci.*, **59**, 420 (1977).
6. R. J. Roe, *J. Phys. Chem.*, **72**, 2013 (1968).
7. A.K. Rastogi and L. E. St Pierre, *J. Colloid Interface Sci.*, **35**, 16 (1971).
8. S. Wu, *J. Phys. Chem.*, **74**, 632 (1970).
9. R. J. Roe, *J. Colloid Interface Sci.*, **31**, 228 (1969).
10. G. L. Gainer, Jr, *Polymer Eng. Sci.*, **12**, 1 (1972).
11. Y. Oh and M. S. Jhon, *J. Colloid Interface Sci.*, in Press.
12. L. A. Girifalco and R. J. Good, *J. Phys. Chem.*, **61**, 904 (1957).
13. H. Eyring and M.S. Jhon, "Significant Liquid Structures", John Wiley, New York, 1969.
14. M.S. Jhon and H. Eyring, "Theortical Chemistry: Advances and Perspectives", Vol. 3, H. Eyring, Ed., Academic Press, New York, 1978.
15. I. Prigogine, N. Trappeniers and V. Mathod, *Disc. Frad. Soc.*, **15**, 93(1953).
16. G.D. Wignall, D.G.H. Ballard and J. Schelten, *Eur. Polymer J.*, **10**, 861 (1974).
17. G.D. Patterson, *J. Macromol. Sci. Phys.*, **B12**, 61(1976).
18. A. A. Askadskkii, *Russ. Chem. Rev.*, **46**, 589 (1977).
19. D. W. VanKrevelen, "Propertics of Polymers", Elsevier, New York, 1972.
20. J. O. Hirschfelder, C. F. Curtiss and R. B. Bird, "Molecular Theory of Gases and Liquids", Chapter 13, John Wiley, New York, 1954.
21. "Handbook of Chemistry and Physics", 57th Ed., R. C. Weast, Ed., CRC Press, Cleveland, Ohio, 1977.
22. T. S. Ree, T. Ree and H. Eyring, *J. Chem. Phys.*, **41**, 524 (1964).

DAEHAN HWAHAK
(*Journal of the*
Vol. 23, No. 4,
Printed in the R

요 약.
Mg-Al eu
位의 平行
이 두
으며 이
sensitivit
값에 따
依存性을
다. 그
났고 또

ABST
(Zn-Al
superpl
two gr
and β_g
our flo
superpl
The
strain
of the
superp
s of t
$+b$ [
each
propo

*Pr

POLYMER SURFACE DYNAMICS

Edited by

J. D. Andrade

The University of Utah
Salt Lake City, Utah

1988

PLENUM PRESS • NEW YORK AND LONDON

DYNAMIC CONTACT ANGLE STUDIES OF N-ALKYL DERIVATIZED BORO-SILICATE GLASS SURFACES

J. M. Park and J. D. Andrade

Department of Materials Science and Engineering
College of Engineering, University of Utah
Salt Lake City, Utah 84112

ABSTRACT

Polymer surfaces and interfaces are mobile and will rearrange or reorient at interfaces to minimize the interfacial free energy with the surrounding phase. As a model system for the study of polymer surface dynamics, we used immobilized n-alkyldimethyl monochlorosilanes (monofunctional) on rigid boro-silicate substrates and compared them with dimethyldichlorosilane (difunctional) treated substrates. Dynamic contact angles were measured by the Wilhelmy plate method as a function of varying alkyl chain lengths, surface concentrations, hydration times, and different solvent environments. In the range of n=4 to n=8, alkyl chains exhibit the minimum advancing contact angle in this system. This suggests that these chains may be relatively more disordered or "liquid-like" than the self-assembling, "crystalline-like", n=18 case, probably due to the low degree of van der Waals interactions possible between the attached intermediate-length chains. The accessibility of water molecules and the shielding effect of the longer chains may contribute significantly to the contact angle difference ($\Delta\theta$). A polymeric layer of difunctional dimethyldichlorosilane (DDS) proved to be a more stable hydrophobic surface compared to a monolayer of monofunctional trimethyl monochlorosilane (TMS). In addition, in an aqueous-methanol solvent environment, the solvation time effect observed is related to alkyl chain lengths.

INTRODUCTION

The dynamics and mobility of polymer surfaces and interfaces is an interesting and practical subject[1,2]. Classical surface chemistry assumes that solid surfaces are rigid and immobile. However, it is expected that polymer molecules in the near surface or interface regions will exhibit motions and relaxations although they are not identical to the motions observed in the bulk due to the different interfacial environment. In general, given

sufficient mobility, polymer surfaces and interfaces can be mobile and the surface can rearrange or reorient at interfaces to minimize the interfacial free energy with the surrounding phase.

The nature of such surface motions is important for biomedical devices[2-4], protein adsorption[5-7] and chromatographic supports[8,9]. The blood compatibility and protein adsorption of biomedical materials depend on their surface properties. We know that the polymer surface in aqueous solution can have different properties than in air or vacuum because of the mobility of polymer surfaces. The chromatographic properties of a reversed phase are dependent upon the conditions of the bonded phases. Understandably, studies of alkyl bonded phases have received considerable attention[10-14]. The motion of such bonded chains is the key to understand their chromatographic properties. Many groups, including Gilpin, et al.[15-17], have investigated dual models of monomeric alkyl surfaces, ranging from a folded or "liquid-like" orientation to a rigid or bristle type in aqueous environment.

In this paper, we apply dynamic contact angle methods to the study of wetting and interfacial phenomena[1,18]. X-ray photoelectron spectroscopy (XPS)[19-21] and attenuated total reflectance (ATR)-Fourier transform infrared (FT-IR) spectroscopy[22,23] also can be used for routine surface studies. FT-IR has the sensitivity to determine the average orientation and reorientation of interfacial chains but does not directly provide information on the motion itself. The mobility of a solute in the neighborhood of an alkyl chain can be measured by fluorescence spectroscopy[24]. Direct measurement of molecular motions and dynamics is offered by ^{13}C NMR studies[25,26] including the spin-lattice (T_1) and the spin-spin relaxation times (T_2). Sindorf and Maciel, et al.[27] investigated the molecular motion of n-alkyl silane bonded to silica particles. In a general sense, the changes in spin-lattice relaxation time (T_1) were consistent with increased segmental motion as a function of distance from the surface. Nagaoka, et al.[7,28] used ^{13}C NMR line widths (which are related to the spin-spin relaxation time (T_2) in order to measure the surface mobility of polyethylene oxide (PEO). The main disadvantage of ^{13}C NMR methods for surface studies is that they are limited to fine particles having high surface areas.

The Wilhelmy plate contact angle method provides a sequential scanning curve or hysteresis loop which can be interpreted in terms of surface mobility, reorientation, solvent penetration and intrinsic wettability, both under water and in air. Although water is a difficult liquid for contact angle studies due to its small molecular volume, resulting in penetration and local swelling of the solid surfaces[29], water is the key component of all biological environments. Therefore we have chosen water as a liquid for contact angle and interfacial studies of biomedical materials.

According to van Damme, et al.[30], the receding contact angles on poly (n-alkyl methacrylates) surfaces decrease in the range of n=6 to n=12, then increase for the n=18. Because of the increasing mobility due to the decreasing T_g, the polymer surfaces with the moderate-length alkyl side chains may reorganize, which may lead to a decreased number of hydrophobic segments exposed to water. In addition, as a minor factor, the hydrophilic ester groups may also reorient toward water surfaces. This result may be closely related to the studies[38] of the brittle temperature for poly n-alkyl acrylates and methacrylates, where they show a minimum in the brittle temperatures in the ranges of n=8 to n=12, due to increased side chain mobility. Alkyl side chain bonded surfaces may have different motions with different chain mobilities. According to C^{13} NMR studies by Sindorf, et al.[27], alkyl chain mobility might increase with chain length (i.e., up to n=8) until the interactions between chains occur at longer chain length (n=18, for example).

It is not easy to measure such alkyl chain lengths effects directly on polymer substrates, because of the packing density problem[31], polymer swelling effects[29] etc. Immobilized alkyl silanes on glass substrates are a good model system for the study of alkyl surface dynamics. Rigid glass surfaces are nondeformable unlike polymer substrates. A rigid glass substrate has very different contact angle than a polymer substrate. Pure clean glass substrates contain silanol groups (i.e., high surface energy) and the contact angles are zero in pure aqueous environment. Hence, we may be sure that the contact angles obtained are indeed due to the alkyl side chains attached to the glass substrates.

The reaction of monofunctional silane reagents with silanol sites at the silica surface results in a single monolayer. Di- and trifunctional silane reagents, especially if water is not completely excluded, hydrolyze and also polymerize, forming a polymeric bonded phase[12].

In this paper a series of n-alkyl dimethyl monochlorosilanes of differing n-alkyl chain lengths (n=1, 4, 8, and 18), available commercially, were bonded on the glass surfaces. In order to study the difference between monomeric surfaces and polymeric surfaces, we used one difunctional silane material, dimethyldichlorosilane (DDS); a well-known hydrophobic surface coating agent.

We studied the effects of different alkyl chain lengths on boro-silicate glass surfaces by varying the surface concentrations and observing the effect of hydration times. In addition, we studied surface interactions with aqueous-methanol mixed solvents.

EXPERIMENTAL

Materials

Trimethyl monochlorosilane (TMS), n-butyldimethyl monochlorosilane (BDS), n-octyldimethyl monochlorosilane (ODS), n-octadecyldimethyl monochlorosilane (ODDS) and dimethyldichlorosilane (DDS) were purchased from Petrarch Systems Inc. (Bristol, PA) and used without further purification (all > 99.5 %). Dimers, present as minor constituents in reagents (for example, $(CH_3)_3SiOSi(CH_3)_3$ for n=1

case), contain no reactive groups. Hence, they should be removed during the rinsing procedure described below.

Pre-purified water was further purified by passing through a Milli-Q reagent water system (Millipore Co.). Toluene (J. T. Baker Chemical Co.) was dried with molecular sieve particles ($Na_{12}[(AlO_2)_{12}(SiO_2)_{12}]\cdot XH_2O$, 4-8 mesh, E. M. Science) for 24 hours before using. Methanol (J. T. Baker Chemical Co.) and dehydrated ethyl alcohol (U. S. Industrial Co.) were used as received.

Corning cover glasses (boro-silicate glasses) 2940, No. 1 1/2, 24 x 50 mm, 0.16-0.19 mm were the glass substrates. As determined by XPS (or ESCA), surface elemental compositions of this boro-silicate glass were for B, Si, O, C; 2.3, 28, 63, 4.4 atom percents, respectively. As minor compositions below 1 %, there are Na, Al, Zn, K, N, and Ti (H is not detected by XPS and is not included).

Methods

Cleaning glass. Glass slides were immersed in chromic-sulfuric acid solution (70mls of saturated aqueous solution of Na_2CrO_4 for each 9 lb bottle H_2SO_4 (J. T. Baker Chemical Co.)) at 80°C for 40 min., which supplied active oxygen atoms that oxidize carbonaceous materials on glass surfaces, rinsed extensively with purified water and then dried overnight in a clean oven at 120°C in air. All other glassware used was also carefully cleaned by the same process.

We examined the cleanliness of the glass slides by measuring the surface tension of purified water (72.6 ± 0.5 dyne / cm) at room temperature (22°C) and by verifying that there was no water contact angle hysteresis and that the slides were perfectly wetted[34]. Cr from cleaning solution was not detected by XPS.

Preparation of monolayer and polymerized layer coatings. Within 30 min., after verifying that the dried slide showed no contact angle hysteresis, clean glass slides were immersed in a suitable concentration of n-alkyldimethyl monochlorosilane in dried toluene and allowed to equilibrate for 15 min. Silanization reaction time was 30 min. for the formation of monolayers at room temperature (22°C)[42]. The slides were then rinsed thoroughly 4-5 times with pure ethanol in order to remove unreacted silane materials. The treated slides were then heated in a vacuum oven at 70°C for 3 hours under nitrogen to remove HCl and ethanol.

DDS coating procedure was same as above except that after 30 min. of silanization, slides were submerged in pure water for about 1 min. to be hydrolyzed, then rinsed with pure ethanol.

The stability of the silane coating on the glass slides was tested by remeasuring the contact angle in purified water after drying in a vacuum oven at room temperature (22°) and by verifying the reproducibility of the contact angle.

Dynamic contact angle measurements. As soon as the coated slides were taken out from the oven and cooled to room temperature, dynamic contact angles were measured by the Wilhelmy plate technique[1,18]. We obtained the wetting curve with an electrobalance (Cahn model RM-2) as a function of the immersion depth[18]. A motor (Motomatic, Electro-craft Co.) drives the shelf to advance or recede the water container at a controlled speed. The chamber is insulated and maintained at room temperature (22°C) and constant humidity (35 % RH).

The output from the electrobalance measurement is fed to an X-Y recorder, with the balance output (force) feeding the Y-axis and immersion depth feeding the X-axis. To measure the advancing and receding contact angle the silane treated glass slides were immersed into or withdrawn from the purified water or mixed solvent at a constant speed of 40 mm / min. Dipping velocity was chosen to be fast enough for convenience of measurement, but slow enough to avoid speed effects (such as hysteresis on the clean glasses). The dipping velocity effect of the silane coated slide by using the Wilhelmy plate method was insignificant .

Hydration time data were measured as follows. One slide was used to measure one time sequence (0, 0.5, 1, 5, 10, and 30 min.). After measuring one time (for example 10 min. of hydration), the slide was dried in a vacuum oven at room temperature (22°C) before the next solvent exposure (for example 30 min.) to remove water or mixed solvent adsorbed on glass surfaces. The reproducibility was examined by remeasuring the contact angle in purified water after drying in a vacuum oven at room temperature (22°C), and by verifying the reproducibility.

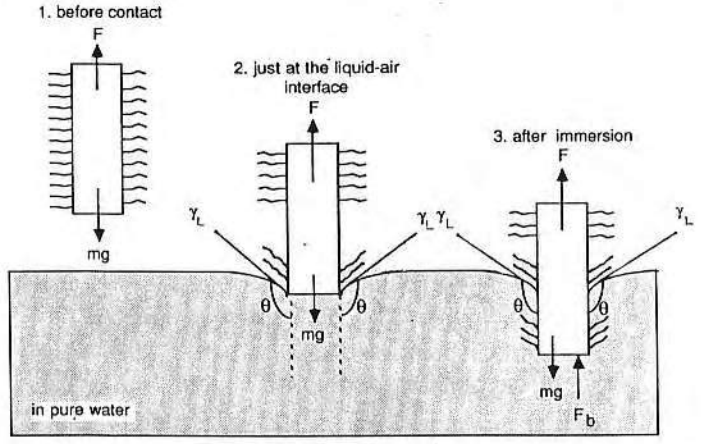

1. $F = mg$
2. $F = mg + p\,\gamma_L \cos\theta$
3. $F = mg + p\,\gamma_L \cos\theta - F_b$

F_b : buoyancy force
p : perimeter of the plate
(for example; n=18 case)

Figure 1. The simplified model of the Wilhelmy plate method with attached long hydrophobic alkyl chains (e.g., n=18) on the glass slide in pure aqueous solution.

Water-methanol solvents were made with an increasing MeOH fraction. Each solution was kept for 15 min. at room temperature (22°C) to equilibrate, then its surface tension was measured.

Figure 1 shows a simplified model of the Wilhelmy plate method showing long hydrophobic alkyl chains attached to the glass surface. We can calculate the contact angle of condition 2, just at the liquid-air interface, by extrapolating to zero depth, thereby eliminating the buoyancy factor, F_b. The contact angle of each sample was measured 3 times. In general, error ranges were within ±3.

RESULTS

Surface Density and Surface Wettability via Functionality

The samples of the different alkyl chain length and the different alkyl surface concentration by varying the silane concentration in the treatment solution were characterized by water contact angle measurements. Advancing and receding contact angles increase with the log of the bulk treatment solution concentration. Figure 2(a) shows the results for monofunctional silane materials (n=1,4, 8 and 18) in the concentration range of 10^{-4} to 0.5 mole / 100 ml toluene (for n=1 and 18 the range was extended to 1.0 mole / 100 ml toluene). In the case of the DDS treatment (Figure 2(b)), the contact angle approached a maximum in the range of near 10^{-2}

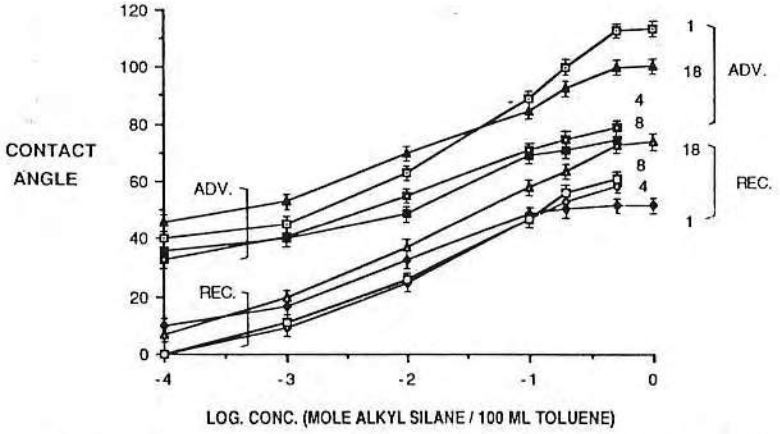

Figure 2(a). Contact angles as a function of alkyl chain length and log concentration (mole / 100 ml toluene); n =1, 4, 8, and 18 (trimethyl monochlorosilane, n-butyl, n-octyl, and n-octadecyldimethyl monochlorosilane); in pure aqueous solution; error bars represent the max. and the min. values of measurements taken from samples prepared at 3 different times. The mean value is the point plotted; ˙: Adv. n=1, ◊:Rec. n=1, ˙:Adv. n=4, ◊:Rec. n=4, ˙:Adv. n=8, ˙:Rec. n=8, Δ:Adv. n=18, Δ:Rec. n=18.

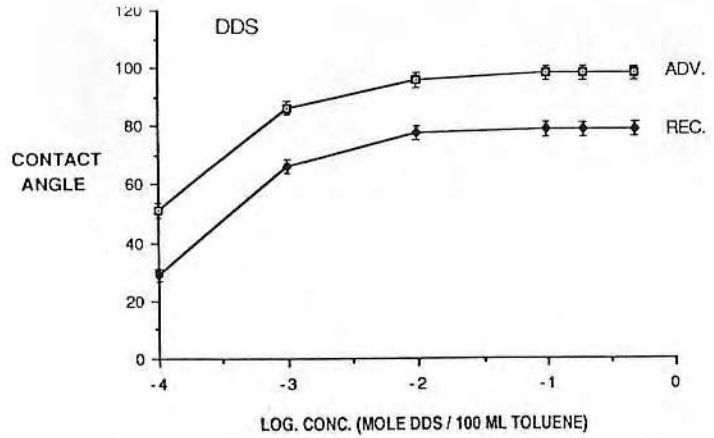

Figure 2(b). Contact angles vs log silane solution concentration (mole/100 ml toluene); DDS (dimethyldichlorosilane) (difunctional); in pure aqueous solution; error bars represent the max. and the min. values of measurements taken from samples prepared at 3 different times. The mean value is the point plotted.

mole / 100 ml toluene. The contact angle data for TMS (monofunctional) and DDS (difunctional) are quite different. Figure 3 shows that in the advancing case TMS is more hydrophobic (113°) than DDS (98°), whereas in the receding case, DDS is more hydrophobic (79°) than TMS (52°). Figure 4 compares the effect of water hydration time for TMS and DDS. The advancing and receding angles for TMS decrease steadily for hydration times up to 30 min.. The advancing and receding angles for the DDS are almost constant, irrespective of hydration time.

The Effect of Alkyl Chain Length on Contact Angle

Figure 5(a) shows that at high surface concentration (0.5 mole alkyl silane / 100 ml toluene), with increasing carbon number the advancing contact angle decreases until n=8, then increase for n=18. Receding contact angles increase continuously with increasing number of carbon atoms. At n=1 the contact angle hysteresis is very large, then decreases until n=8. At n=18, however, it increases again but less than that of n=1.

Figure 5(b) shows the low surface concentration condition (10^{-2} mole / 100 ml toluene). Generally, the contact angles are reduced compared to the above high surface concentration condition and both advancing and receding contact angles show the same trend, i.e., both angles decrease until n=8 and then increase again.

The Effect of Hydration Time on The Water Contact Angle

Contact angle difference ($\Delta\theta$) is defined as the contact

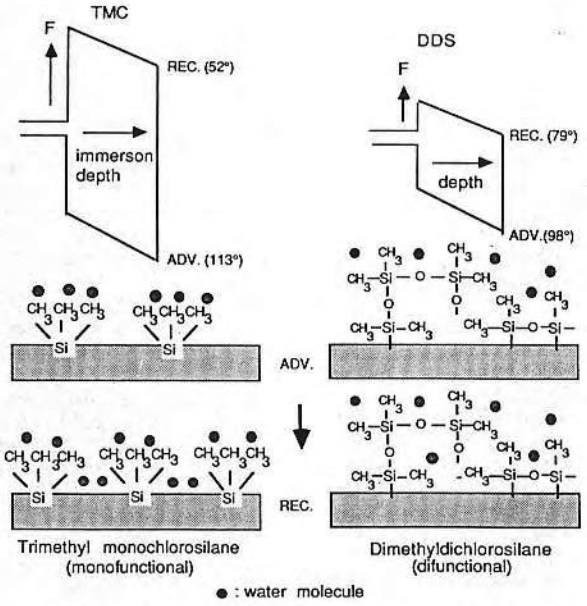

Figure 3. Models for water interaction with trimethyl monochlorosilane (TMS) (monofunctional) and dimethyldichlorosilane (DDS) (difunctional and polymerized) surfaces. Water can readily interract with the glass surfaces in the TMS case (left figure) while the polymerized DDS coating restricts water penetration (right figure).

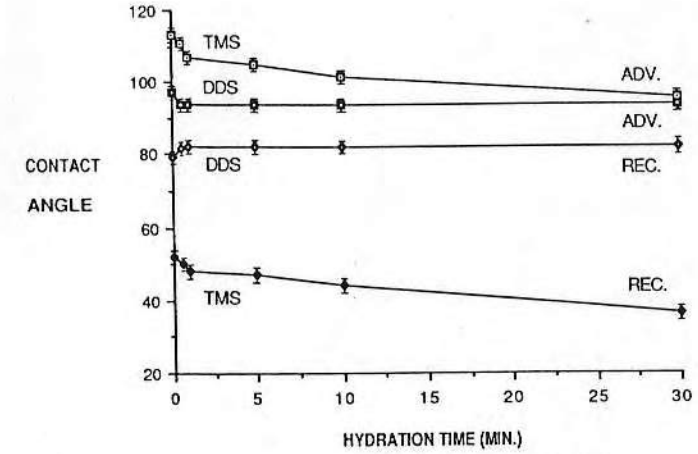

Figure 4. Contact angles of TMS (monolayer) and DDS (multilayer) with increasing hydration time (min.) at high surface concentration (0.5 mole / 100 ml toluene); error bars represent the max. and the min. values of measurements taken from samples prepared at 3 different times. The mean value is the point plotted.

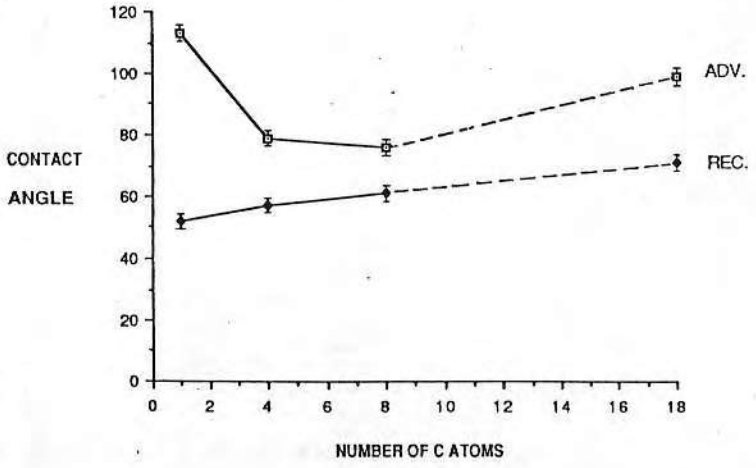

Figure 5(a). Chain length effect at high surface concentration; concentration: 0.5 mole alkyl silane / 100 ml toluene; in pure aqueous solution; error bars represent the max. and the min. values of measurements taken from samples prepared at 3 different times. The mean value is the point plotted.

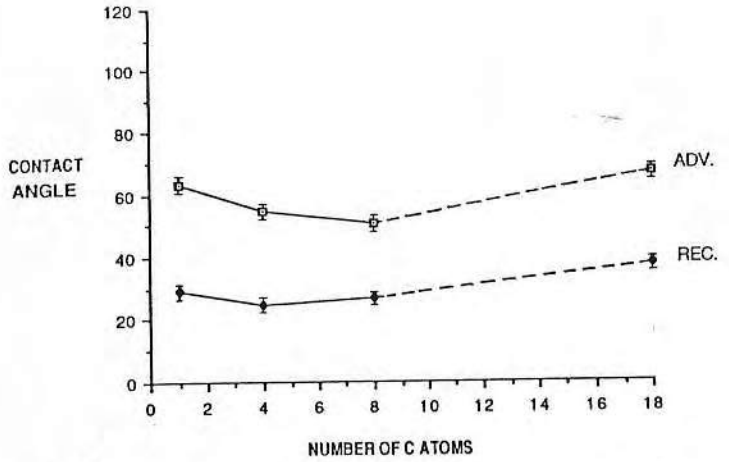

Figure 5(b). Chain length effect at low surface concentration; concentration: 10^{-2} mole alkyl silane / 100 ml toluene; in pure aqueous solution; error bars represent the max. and the min. values of measurements taken from samples prepared at 3 different times. The mean value is the point plotted.

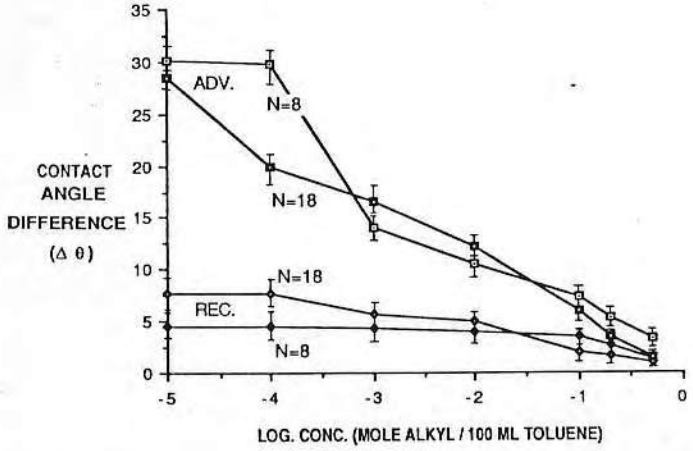

Figure 6(a). Contact angle difference ($\Delta\theta$) with increasing concentration (mole alkyl silane /100ml toluene); hydration time: 30min.; n = 8, 18; in pure aqueous solution; $\Delta\theta$ = the initial contact angle (0 min.) - the final contact angle (30 min.); error bars represent the max. and min. values of measurements taken from samples prepared at 3 different times. The mean value is the point plotted.

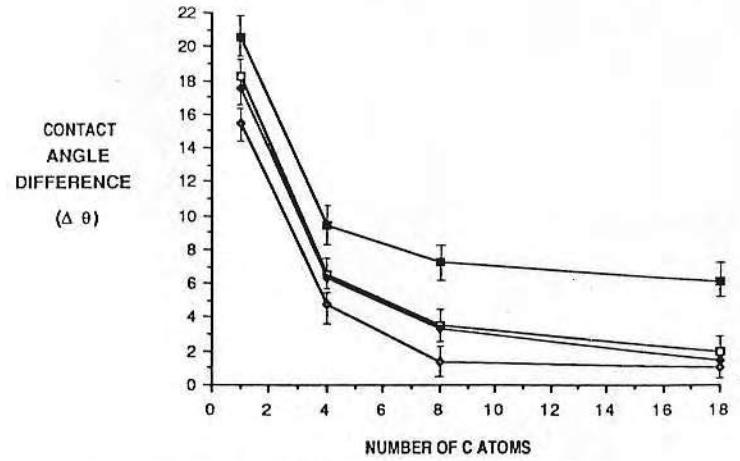

Figure 6(b). Contact angle difference ($\Delta\theta$) with increasing number of C atoms, hydration time: 30 min.; concentration: 0.5, 0.1 mole alkyl silane /100 ml toluene; in pure aqueous solution; Δq = the initial contact angle (0 min.) - the final contact angle (30 min.); error bars represent the max. and the min. values of measurements taken from samples prepared at 3 different times. The mean value is the point plotted; ◊ Adv., conc.:0.5, ◊ Rec., conc.:o.5, · Adv, conc.:0.1, · Rec., conc.:0.1

angle at 0 min. hydration time less the contact angle at 30 min. hydration time. Figure 6(a) shows that at longer chain lengths (n=8 and 18), the contact angle difference decreases with increasing silane treatment solution concentration. This trend is most significant in the advancing angle case. On the other hand, as shown in Figure 6(b), we can see that as the chain length increases the contact angle difference decreases at high and low concentrations (i.e., 0.5 and 0.1 mole / 100 ml toluene).

<u>The Effect of Water-Methanol Mixed Solvent Environments on the Contact Angles</u>

Figure 7 presents the H_2O-MeOH surface tension as a function of MeOH concentration measured at 20°C by the Wilhelmy plate technique using clean glass plates. In Figure 8, both contact angles decreases to zero (meaning perfect wetting) with increasing MeOH concentration, as expected, except for n=1.

In Figure 9(a) we studied elapsed time for up to 10 min. for a H_2O : MeOH = 75 : 25 environment. The contact angle is nearly constant with increase in elapsed time for the n=1 and 18 cases, whereas for the n=4 and 8 cases the contact angle decreases. Figure 9(b) shows that as the MeOH fraction increases, the initial decrease of contact angle increases up to 50 % MeOH, then it is almost same until 75 % MeOH. After 1 min. of contact the angle is constant because the alkyl chain is saturated with methanol molecules.

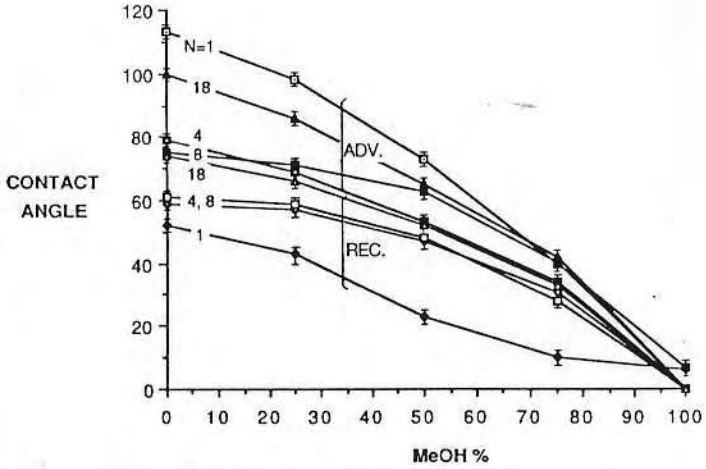

Figure 7. Surface tension of H_2O : MeOH mixed solvent at room temperature (22°C); error bars represent the max. and the min. values of measurements taken from solutions prepared at 3 different times. The mean value is the point plotted.

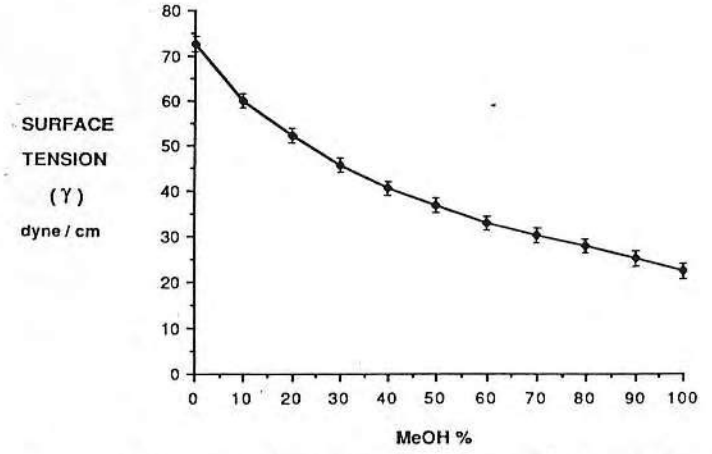

Figure 8. Mixed solvent effect for n=1, 4, 8, and 18 at high concentration (0.5 mole alkyl silane / 100 ml toluene); elapsed time: 0 min.; error bars represent the max. and the min. values of measurements taken from samples prepared at 3 different times. The mean value is the point plotted.

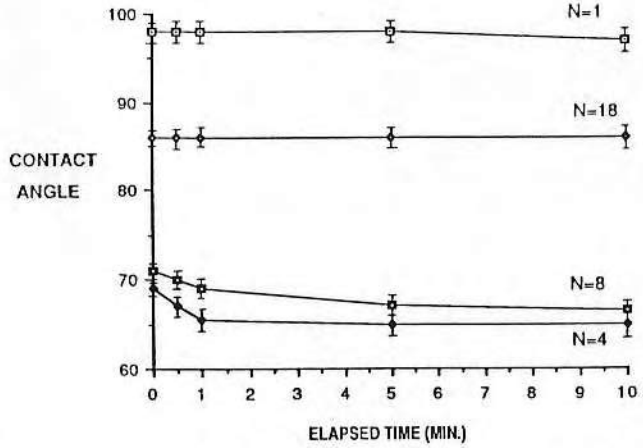

Figure 9(a). Advancing contact angles for n=1, 4, 8, and 18 in mixed solvent (H_2O : MeOH = 75 : 25) as a function of elapsed time (10 min.) in the mixed solvent; error bars represent the max. and the min. values of measurements taken from samples prepared at 3 different times. The mean value is the point plotted.

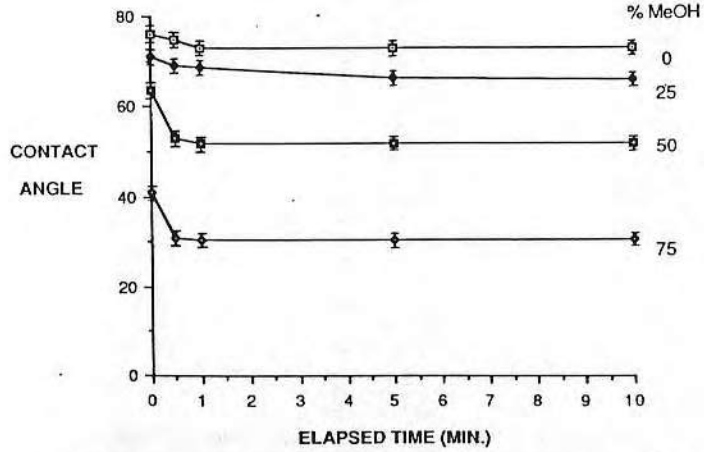

Figure 9(b). Advancing contact angles of different MeOH ratio at high concentration (0.5 mole ODS / 100 ml toluene) as a function of elapsed time (10 min.); n=8; error bars represent the max. and the min. values of measurements taken from samples prepared at 3 different times. The mean value is the point plotted.

DISCUSSION

Surface Density and Surface Wettability vs Functionality

In the model system used we may change relatively the surface concentration by preparing the samples with different silane solution concentrations. As seen in Figure 2(a) both advancing and receding contact angles increase with increasing silane bulk solution concentration. At low concentration, there may be less surface density and the surface may be nonuniform or "island-typed"[16, 39]. The predominance of the hydrophilic silanol phase causes low contact angles. At high concentration the bonded alkyl chains are more prevalent and probably are relatively densely-packed with the higher silane solution concentrations used. Contact angle curves for the monofunctional bonded phases (n=1, 4, 8 and 18) in the pure aqueous environment show that the hydrophobicity increases almost linearly up to 0.5 mole alkyl silane concentration. Above 0.5 mole concentration, the rate of increase is reduced remarkably.

In the difunctional bonded phase (DDS) case the curve plateaus at a much lower concentration (Figure 2(b)). We can explain this trend as follows. Due to difunctionality, the silane materials may polymerize. Thus near the 10^{-2} mole conc. the minimum concentration for hydrolysis is already present and polymerization may occur. The contact angle reaches a maximum because the polymerized phase may shield the hydrophilic silanol groups, giving the surface a hydrophobic character. These two different curves in Figures 2(a) and (b) suggest that monofunctional silane materials may produce monolayer surfaces, whereas difunctional silane materials may give polymeric surfaces.

As seen in Figure 3, the advancing contact angle on TMS (monofunctional) shows a slightly larger hydrophobicity (i.e., by about 15°) than that of DDS (difunctional). In the TMS case, the surface consists of rigid, short, monomeric units. The monomeric TMS coated surfaces may contain three exposed hydrophobic methyl groups packed tightly per silane unit. In the case of the polymerized DDS coated surfaces, multilayers are probably present. Therefore, the outermost surface has a decreased number (i.e., decreased density) of methyl groups, resulting in a lower contact angle. In the receding contact angle, the difference in angle between TMS and DDS is 27°, which is quite large. Figure 3 suggests that water molecules can penetrate and interact with remaining hydrophilic silanol groups. When the receding process begins, surfaces are wetted well with water molecules which have penetrated to the silanol sites. Surface heterogeneity also may contribute to a large contact angle hysteresis for TMS[40].

The advancing (113°) and receding angles (52°) for TMS in this work were different from those reported by Ralston, et al.[34] (88° and 72°, respectively). The reason for these differences may be due to this factor: Ralston et al. used pure-silica plates and particles, whereas we used boro-silicate glass substrates, which have a higher surface reactivity than does pure-silica[35]. In general, boro-silicate glasses are known to react with silane materials more strongly than pure-silica due to boron ions which attract electrons from neighbouring silanol groups. Hence, they not only increase the Brönsted acid strength of boron groups but also enhance the reactivity of neighbouring silanol groups. Greater amounts of TMS attached to boro-silicate glass surfaces compared to silica surfaces may increase the advancing contact angle. As minor factor, different methods of contact angle measurement may cause the contact angles to be slightly different[36, 45]: we used Wilhelmy plate technique, whereas they used captive-bubble and sessile-drop techniques.

In Figure 4, we can see the phenomenon as a function of hydration times. In TMS, as the hydration time increases, both contact angles decrease, whereas in DDS, the contact angles are almost constant with hydration time. In the case of monomeric TMS, the water molecules may penetrate easily through the monomeric short alkyl chains. The accessibility of water is limited to a large extent in the polymeric DDS, probably due to the polymerized multilayer, hence, hysteresis is small and contact angles are almost constant with hydration times. This is the reason why we usually use DDS-coated surfaces as model hydrophobic surfaces in our biomedical studies, because it is stable with time, in spite of having a lower hydrophobicity than the TMS surface.

Factors Affecting Contact Angles

There are four factors governing the exact nature of alkyl chain surfaces. First, as already seen in the previous figures, the monomeric or polymeric nature of the film depends on the functionality of the silane materials. Second, the degree of silanization and the surface concentration may influence the accessibility of water molecules to the unreacted hydrophilic silanol groups remaining on the underlying glass surfaces.

Third, the length of the alkyl chain is a main factor in this work. It is expected that for the moderate chain lengths, the chains are relatively mobile[27, 30]. There are interactions between the chains (i.e., van der Waals forces) at long chain lengths[41]. These different chain types (e.g., "folded" and "extended") may affect contact angles due to the different outermost groups exposed (e.g., CH_3- and $-CH_2-$)[32]. According to I.R. spectroscopic and ellipsometric studies by Porter, et al.[44], the long n-alkyl thiols (about n=18) form a densely-packed, "crystalline-like" assembly with fully extended alkyl chains. As the alkyl chain length decreases, the surface structure becomes increasingly disordered, "liquid-like" with lower packing density and coverage. Fourth, the effect of an aqueous environment is different from that of the aqueous-methanol solvent environment. Though we usually use water for biomedical studies, for chromatographic studies the mixed solvent is very important. In a mixed solvent environment, the bonded alkyl chain can be "bristle" or "brush-like"[15-17].

In Figure 5(a), the advancing angle decreases until n=8 then increase for the n=18 case. Contact angle data are not presented for chain lengths in the range between n=8 and n=18, because silanes of these lengths were not available

commercially. The van der Waals forces between these chain lengths (for example, n=12, 14, 16) may be expected to increase continuously up to n=18, well known to be capable of self-assembly[43, 44]. According to Johnson and Dettre[37], the advancing contact angle is associated with the low surface energy region (i.e., high contact angle). We can tell that the advancing angle may depend on the total hydrophobicity of surfaces, which also depends on the number and the chain length of hydrophobic alkyl groups (i.e., CH_3- and -CH_2-) in the silane molecules adsorbed on the surfaces. ^{13}C NMR studies[27] show that the motion of terminal methyl carbons of n-alkyldimethyl monochlorosilanes on silica particles increases until n=8, then at n=18 it becomes almost constant.

Now, we analyze our trends in Figure 5(a) in two steps: the first is the silanization procedure in toluene solution; the second is the contact angle measurement in aqueous environment. In the n=1 case, silane molecules can bind to reactive sites on the glass surfaces in a densely-packed state, probably due to the bulky three methyl groups per silane molecule. For the longer n=4 and 8 cases (e.g., their chain lengths are 0.71 and 1.20 nm, respectively), the adsorbed amount may decrease slightly until n=8, probably due to an increased excluded-volume effect. Therefore the mean distances between chains may increase with n. In the n=18 case (i.e., chain length is 2.47 nm), the adsorbed surfaces may be more densely-packed due to van der Waals forces between the long chains.

During measurement of contact angles, the expected behavior of hydrophobic alkyl chains in an aqueous environment is as follows. In the case of n=1, because water molecules contact their rigid, hydrophobic, methyl groups on the top of the surfaces, they exhibit a high advancing angle. The receding angles are much lower, probably due to the easy penetration of water molecules to the unreacted silanol groups and to possible surface heterogeneity. Therefore the contact angle hysteresis is large.

In n=4 case, the advancing angle is lower than that of n=1. Due to the folded style in aqueous environment[15], it may expose many methylene groups on the top of the surfaces. We know that methyl group has a lower critical surface tension (i.e., 24 dynes / cm) than that of methylene group, 31 dynes / cm [32]. Therefore water molecules may touch methylene groups in chains, resulting in the contact angle to be lower. In n=8 case, general trend is similar to n=4 case. However, the increased methylene numbers in a chain cause the advancing angle to decrease slightly. In addition, slightly decreased silane amounts attached may contribute to the decreased contact angles until n=8. For such moderately longer alkyl chains (i.e., n=4 and 8), due to the low degree of van der Waals interactions possible between the attached intermediate-length alkyl chains, there may be an excluded-volume for the folded alkyl chains to be relatively more mobile, disordered, and "liquid-like" than the self-assembling, "crystalline-like," n=18 case. On the other hand, the contact angle hysteresis decreases until n=8, probably due to the excluded-volume and the shielding effect of the folded chains (i.e., n=4 and 8) against water molecules approaching glass surfaces.

In the case of n=18, the advancing angle increases again. Due to alkyl chain interaction and packing, the water molecules may touch only the outermost alkyl chain methyl groups on the top of the surfaces, meaning that the water molecules find it difficult to penetrate into the silane bundles, giving less chances to contact methylene groups inside bundles. Hence, the advancing angle is high for n=18.

In Figure 5(b), the general shapes are similar to those trends shown in Figure 5(a) except for the case of n=1. Due to the lower concentration of the hydrophobic alkyl chain, the contact angles are generally lower. A unique difference between Figures 5(a) and 5(b) can be seen if one considers receding contact angles. At low concentrations of alkyl silane (Figure 5(b)), the contact angle hysteresis for the n=1 case is smaller than that of the high concentration of alkyl silane (Figure 5(a)). This is because a large fraction of the glass surfaces may have exposed the hydrophilic silanol sites and is not subject to penetration by the water molecules through alkyl chains, resulting in a smaller contact angle hysteresis. A minimum near n=4 and 8 is again observed like Figure 5(a); hence, we believe that at low surface coverages, the chain may be mobile and adopt folded styles at n=4, n=8. At the long chain length n=18, these insufficiently covered surfaces form partially ordered island-type rather than a homogeneous layer[39]. Water molecules may contact most of methyl groups on the top of these island-typed surfaces rather than methylene groups. Therefore as in the high concentration case, contact angle increases again at n=18.

In Figure 6(a), the contact angle difference ($\Delta\theta$) represents the change in contact angle after 30 min. hydration time: the initial contact angle (0 min.) - the final contact angle (30 min.). The contact angle difference ($\Delta\theta$) can tell us that many water molecules may access the hydrophilic silanol surfaces during 30 min. At longer chain lengths (i.e., n=8 and 18), the advancing angle difference ($\Delta\theta$) decreases steeply with increasing silane solution concentration. At low concentration (i.e., hydrophilic portions dominate), because the longer chains may not shield the whole surfaces still containing many remaining silanol groups. Therefore, water molecules may access these silanol surfaces, resulting in the larger contact angle difference ($\Delta\theta$). Whereas at high concentration (i.e., hydrophobic portions dominate), the longer chains can shield the surfaces relatively well, the water molecules may not be allowed to access the small remaining silanol groups, causing the contact angle difference ($\Delta\theta$) to be small. This may also be related to the heterogeneity of such a surface.

Figure 6(b) shows the effects of chain length at high and low silane solution concentrations. The contact angle difference ($\Delta\theta$) is defined in the same way as Figure 6(a). As the chain length increases, both the contact angle differences ($\Delta\theta$) decrease sharply between n=1and n=4, then decrease steadily for n=18. From this figure we can deduce that the longer the chain, the larger the shielding effect. In the case

of n=1, the contact angle difference ($\Delta\theta$) is large due to its short, rigid monolayer, and easy penetration of water molecules, as mentioned previously. In the n=18 case, these long alkyl chains may have a much higher shielding effect causing the contact angle difference ($\Delta\theta$) to be small. Because the n=18 case is a densely-packed bundle-type due to the high degree of van der Waals interactions, the penetration of water molecules is more difficult.

We usually use only water as a solvent for the study of biomedical materials. However in other applications, for example, reversed-phase liquid chromatography, different solvents are used, such as water-methanol mixed solvents. As the MeOH fraction increases, the surface tension decreases (Figure 7). The general trend is as follows. In an aqueous environment, the alkyl chain is "folded" and shows the hydrophobicity, whereas in aqueous-methanol solvent environment the chain is "brush-like" or "extended" as stated by Halasz and Sebestian[17]. Due to lower surface tensions of mixed solvents, contact angles are lower. In Figure 8, as the MeOH fraction increases, both contact angles decrease steadily to the angle 0° except for the n=1 case, where even with a pure MeOH environment, contact angles approach 10° due to the large hydrophobicity.

In Figure 9(a), for the condition of the 25 % MeOH fraction, we can observe interesting solvation time effects as a function of chain length and elapsed time. In the case of n=4, contact angles decrease steeply up to about 1 min. Whereas, in the n=8 case the contact angles decrease steadily up to 5 min.. This means that in the n=4 case, it may takes a relatively short time to solvate. The longer n=8 chain probably requires a longer time for solvation than that of n=4[13].

On the other hand, for the n=1 case, unlike the aqueous environment (i.e., from Figure 6(b), the contact angle difference ($\Delta\theta$) is the largest), the solvation time may be too short to observe, because MeOH molecules have the same hydrophobic nature with methyl groups of short chain length on the surfaces. Hence, it looks constant, meaning that the contact angle difference ($\Delta\theta$) for 10 min. elapsed time is almost zero. However, even though the shape of the line for the case of n=18 is also linear, the reason may be different from that of the n=1 case. Because the bundle-type due to the high degree of van der Waals interactions, much longer chain attached surfaces seldom allow methanol molecules to penetrate. With respect to the chain length effect, these trends in Figure 9(a) probably are correlated to the results of Figure 6(b) in the aqueous environment.

In Figure 9(b), at the initial stage, in the 0 and 25 % methanol cases, the contact angles decrease steadily, whereas for 50 and 75 % methanol, the contact angles drop steeply up to 0.5 min.. In addition, at 50 % MeOH, the contact angle drop is almost the same as that of 75 % MeOH. We can deduce that beyond 50 % MeOH the surfaces are already saturated with methanol molecules, hence the solvation time decreases within about 0.5 min. for 50 and75 % cases.

CONCLUSIONS

Dynamic contact angles in water and water-methanol solvents vary with chain lengths, surface concentrations, and hydration times for n-alkyldimethyl monochlorosilanes (i.e., n=1, 4, 8, and 18) and dimethyldichlorosilane treated surfaces as measured by the Wilhelmy plate method.

1. For both high and low surface concentrations, monomeric alkyl silanes in the ranges of n=4 to n=8 exhibit the minimum advancing contact angle. This suggests that these chains may be relatively more disordered or "liquid-like" than the self-assembling, "crystalline-like", n=18 case. This is probably a result of an excluded-volume effect due to the low degree of van der Waals interactions possible between the attached intermediate-length chains.

2. With increasing silane solution concentration, the contact angle difference ($\Delta\theta$) decreases because the penetration of water molecules may decrease, and which results in increasing hydrophobicity. In addition, with increasing chain lengths, the contact angle difference ($\Delta\theta$) decreases, probably due to the shielding effect of the longer chains.

3. A polymeric layer of difunctional dimethyldichlorosilane (DDS) proved to be a more stable hydrophobic surface compared to a monolayer of monofunctional trimethyl monochlorosilane (TMS).

4. In the mixed solvent environment, the solvation-time effect observed was related to alkyl chain lengths. For the n=1and 18 cases, there was no solvation-time, whereas for the n=4 and 8 cases, a short solvation time was observed.

ACKNOWLEDGEMENTS

We thank Dr. W. Bascom, Dr. J. Kopecek, Dr. S. Garoff, and Dr. H. Ringsdorf for their helpful discussions on the model system of alkyl chains on glass surfaces and on the topic of the surface concentration. We also thanks Mr. J-H Lee and Mr. P. Dryden for their discussions on the thermodynamic aspects of contact angles.

REFERENCES

1. J. D. Andrade, D. E. Gregonis, ane L. M. Smith, Chapter 2. "Polymer surface dynamics," in "Surface and Interfacial Aspects of Biomedical Polymers," J. D. Andrade ed., 15, Plenum Press (1985).
2. H. Yasuda, A. K. Sharma and T. Yasuda, "Effect of orientation and mobility of polymer molecules at surfaces on contact angle and its hysteresis," J. Polym. Sci. Polym. Physics, 19, 1285 (1981).
3. R. S. Ward Jr., "Development of thermoplastics," Organic Coatings and Plastics Preprints, 42, 227 (1980).
4. J. D. Andrade, "Contact angle analysis of biomedical polymers: From air to water to electrolytes," in "Polymers

in Medicine II," E. Chiellini, et al., ed., 29, Plenum Press (1986).
5. E. W. Merrill, and E. W. Salzman, V. Sa da Costa, D. Brier-Russell, A. Dincer, P. Pape, J. N. Lindon, "Platelet retention on polymer surfaces. Some in vitro experiments," Adv. Chem. Series, 199, 35 (1982).
6. D. E, Gregonis, D. E. Buerger, R. A. Van Wagenen, S. K. Hunter, and J. D. Andrade, " Poly (ethylene glycol) surfaces to minimize protein adsorption," Second World Congress on Biomaterials, abstracts, 266 (1984).
7. S. Nagaoka, Y. Mori, H. Takiuchi, K. Yokota, H. Tanzawa, and S. Nishumi, "Polymers as Biomaterials," S. W. Shalaby, A. S. Hoffman, B. D. Ratner and T. A. Horbett, ed., 361, Plenum Press (1984).
8. Z. Kessaissia, E. Papirer and J. B. Dommet, "Molecular transitions of alkyl chains grafted onto silicas observed by gas chromatography," J. Colloid Interface Sci., 79, 257 (1981).
9. R. K. Gilpin, "The bonded phase: structure and dynamics," J.Chromatographic Sci., 22, 371 (1980).
10. L. C. Sander and S. A. Wise, "Synthesis and characterization of polymeric-C18 stationary phases for liquid-chromatography," Anal. Chem., 56, 504 (1984).
11. P. Roumeliotis and K. K. Unger, "Structure and properties of n-alkyldimethylsilyl bonded silica reversed-phase packings," J. Chromatography, 149, 211 (1978).
12. L. C. Sander, J. B. Callis and L. R. Field , "Fourier-transform infrared spectrometric determination of alkyl chain conformation on chemically bonded reversed-phase liquid-chromatography packings," Anal. Chem., 55, 1068 (1983).
13. C. R. Yonker, T. A. Zwier and M. F. Burke, "Comparision of stationary phase formation in R.P- for methanol-water systems," J. Chromatography, 241, 257 (1982).
14. K. Karch, I. Sebestian and I. Halasz, "Preparation and properties of reversed phases," J. Chromatography, 122, 3 (1976).
15. R. K. Gilpin and J. A. Squires, "Effect of temperature on the orientation of bonded hydrocarbon phases in totally aqueous liquid chromatographic systems," J. Chromatograpic Sci.,19, 195 (1981).
16. C. H. Lochmuller and D. R. Wilder, "The sorption behavior of alkyl bonded phases in reversed-phase, high performance liquid chromatography," J. Chromatographic Sci., 17, 574 (1979).
17. I. Halasz and I. Sebestian, "New stationary phase for chromatography," Angrew. Chemie Int. Ed. Engl., 8, 453 (1969).
18. J. D. Andrade, S. M. Ma, R. N. King and D. E. Gregonis, "Contact angles at the solid-water interface," J. Colloid Interface Sci., 72, 488 (1979).
19. J. D. Andrade, Chapter 5. X-ray Photoelectron Spectroscopy (XPS) in "Surface and interfacial aspects of biomedical polymers," J. D. Andrade ed.,105, Plenum Press (1985).
20. A. D. Baker, ed., "Electron Spectroscopy: Theory, Techniques and Applications," Vol. 2, Acad. Press (1981).
21. K. Keller, ed., chapter IV, "Surface Characterization," in "Guidelines for Physicochemical Characterization of Biomaterials," NIH Publ., No. 80-2186, 33 (1980).
22. E. J. Castillo, J. L. Koenig, C. K. Kliment and J. Lo, "Surface analysis of biomedical polymers by ATR FT-IR," Biomaterials, 5, 186 (1984).
23. S. R. Holmes-Farley, R. H. Reamey, T. J. McCarthy, J. Deuch, and G. M. Whitesides, "Acid-base behavior of carboxylic acid groups covalently attached at the surface of polyethylene: The usefulness of contact angle in following the ionization of surface functionality," Langmuir, 1, 725 (1985).
24. C. H. Lochmuller, A. S. Colborn, M. L. Hunnicutt, and J. M. Harris, "Bound pyrene excimer photophysics and the organization and distribution of reaction sites on silica," J. Am. Chem. Soc., 106, 4077 (1984).
25. L. Faccini, A. P. Legrand, "Nuclear magnetic resonance study of the segmental motion of poly (ethylene oxide) 2000 grafted on silica," Macromolecules, 17, 2405 (1984).
26. G. C. Levy, P. L. Rinaldi, J. J. Dechter, D. E. Axelson, L. Mandelkern, "Molecular dynamics of polymer chains and alkyl groups in solution," J. Am. Chem. Soc., 20, 119 (1980).
27. D. W. Sindorf, G. E. Maciel, "C-13 CP/MAS NMR-study of molecular motion in normal-alkylsilanes bonded to the silica surface," J. Am. Chem. Soc., 105, 1848 (1983).
28. S. Nagaoka, Y. Mori, H. Takiuchi, K. Yokota, "Interaction between blood components and hydrogels with poly (oxyethylene) chain," Polymer Preprints, 24, 67 (1983).
29. C. O. Timmons and W. A. Zisman, "Effect of liquid structure on contact angle hysteresis," J. Colloid Interface Sci., 22,165 (1966).
30. H. S. van Damme, A. H. Hogt and J. Feijen, "Surface mobility and phase transitions of poly (n-alkyl methacrylates) probed by contact angle measurements," J. Colloid Interface Sci., 114, 167 (1986).
31. J. J. Kirkland, "Microparticles with bonded hydrocarbon phases for high performance reverse-phase liquid chromatography," Chromatographia, 8, 661 (1975).
32. W. A. Zisman, "Relation of equiliurium contact angle to liquid and solid constitution," in "Contact Angle, Wettability, and Adhesion," R. F. Gould ed., Adv. Chem. Series, 43, 1 (1964).
33. L. Smith, C. Doyle, D. E. Gregonis, and J. D. Andrade, "Surface oxidation of cis-trans polybutadiene," J. Appl. Polym. Sci., 26, 1269 (1982).
34. R. Crawford, L. K. Koopal, and J. Ralston, "Contact angles on particles and plates," Colloids and Surfaces, (1987), in press.
35. M.L. Hair and W. Hertl, "Reactivity of boria-silica surface hydroxyl groups," J. Phys. Chem., 77, 1965 (1973).
36. G. E. P. Elliott and A. C. Riddiford, "Dynamic contact angles, I. The effect of impressed motion," J. Colloid. Interface Sci., 23, 389 (1967).
37. R. E. Johnson and R. H. Dettre, "Wettability and contact angles," in "Surface and Colloid Science," E. Matijevic ed., 2, 85 (1969).
38. C. E. Rehberg and C. H. Fisher, "Properties of monomeric and polymeric alkyl acrylates and methacrylates," Industrial and Eng. Chem., 40, 1429 (1948).
39. S. Garoff, H. W. Deckman and M. S. Alvarez, Proceedings-Electrochem. Soc., 85-8, 112 (1985).
40. L. W. Schwartz and S. Garoff, "Contact angle hysteresis on heterogeneous surfaces," Langmuir, 1, 219 (1985).
41. O. Levine and W. A. Zisman, "Physical properties of monolayers adsorbed at the solid-air interface. I. Friction and wettability of aliphatic polar compounds and effect of

halogenation," J. Phys. Chem., 61, 1068 (1957).
42. J. Gun and J. Sagiv, "On the formation and structure of self-assembling monolayers. III. Time of formation, solvation, and release," J. Colloid Interface Sci., 112, 457 (1986).
43. O. Levine and W. A. Zisman, "Physical properties of monolayers adsorbed at the solid-air interface. I. Friction and wettability of aliphatic polar compounds effect of halogenation," J. Phys. Chem., 61, 1068 (1957).
44. M. D. Porter, T. B. Bright and D. L. Allara, "Spontaneously organized molecular assemblies. 4. Structural Characterization of n-alkyl thiol monolayers on gold by optical ellipsometry, infrared spectroscopy and electrochemistry," J. Am. Chem. Soc., (1987), in press.
45. D. E. Gregonis, R. Hsu, D. E. Buerger, L. M. Smith, and J. D. Andrade, "Wettability of polymers and hydrogels as determined by Wilhelmy plate technique," in "Macromolecular Solutions," R. B. Seymour and G. A. Stahl, eds., 121, Pergamon Press (1982).

Original

HEMOGLOBIN ADSORPTION ONTO ALKYL AGAROSES

by

J. M. Pierce*, J. D. Andrade+, and
D. E. Gregonis
Department of Bioengineering
University of Utah
Salt Lake City, Utah 84112

*Sorenson Research, Inc.
4455 Atherton Drive
Murray, Utah 84107

+To whom correspondence and reprint requests should be addressed

Submitted by J. M. Pierce in partial fulfillment of the requirements for the M. Sc. degree in Bioengineering, University of Utah.

Submitted to J. Colloid and Interface Science, July, 1983.

ABSTRACT

The differently liganded hemoglobins, cyano-hemoblogin (HbCN), oxygenated hemoglobin (HbO_2), and deoxyhemoglobin (deoxy-Hb) show different adsorption characteristics from pure solutions onto alkyl agaroses. At concentrations comparable to those which may exist in vivo under conditions of localized hemolysis, HbO_2 and deoxy-Hb show differences in adsorption on artificial surfaces that may suggest preferential adsorption to devices in the circulatory system.

Adsorption isotherm break points occur at approximately constant levels of adsorption and seem to be a characteristic of the particular liganded hemoglobin in the concentration range being examined. The affinity of adsorption appears to be mediated by a combination of hemoglobin ligand type and alkyl ligand density.

INTRODUCTION

Protein adsorption to the surfaces of materials exposed to blood plays a pivotal role in subsequent cellular interactions. The adsorption of hemoglobin (Hb) warrants study if either the plasma Hb concentration can become elevated, or if adsorption of Hb may be strongly preferred over that of other plasma proteins. Hemoglobin adsorption is not usually considered in plasma (or blood) protein adsorption studies as the plasma concentration of Hb is small compared to that of albumin, fibrinogen, γ-globulins, and the other common plasma proteins. Hemoglobin is 0.01% or less of the total protein mass in plasma, under normal conditions.

Red blood cells live approximately 120 days, and abnormal cells are removed by three general mechanisms: 1) sequestered by the spleen for mild abnormalities, 2) liver removal of more severely damaged cells, 3) intravascular lysis. Gross injury to the erythrocyte, such as those induced by trauma or complement, result in red cell destruction in the intravascular space, as during surgical trauma upon implantation. Plasma Hb concentration can rise rapidly in those situations due to hemolysis.

Haptoglobin (Hp) readily binds irreversibly to extracorpuscular plasma Hb dimer. The Hb-Hp complex is too large to filter across the glomerulus, but instead is taken up by hepatic parenchymal cells. When Hp sites are saturated, free Hb passes into the

glomerular filtrate. Haptoglobin synthesis is not increased in hemolytic states.

Horbett et al. have shown high affinity adsorption of Hb to polyethylene surfaces (1-3). Adsorption data of Hb to other artificial surfaces is very limited (4-11). Most literature on Hb is based on intravascular interactions (12) and ligand interactions. Consequently, much is known about the structure and properties of Hb, but little about its adsorption behavior. The work of Gendreau, et al., on direct flowing blood interactions with Germanium plates by Fourier transformation infrared (FTIR) spectroscopy technique, suggests that Hb adsorption may be occurring during the very early stages of blood contact (13).

Hemoglobin exists in the red cell as a hydrophobically bound tetrameric unit. In plasma, Hb dissociates to the dimer form and as such displays hydrophobic patches on its surface.

Hydrophobic substrates were chosen to study the adsorption of Hb. For hydrophobic substrates, alkyl agaroses, as employed in hydrophobic chromatography, were used. Hydrophobic chromatography has proven to be quite sensitive as a separation tool. The hydrophobicity of the binding sites is controlled by both the ligand hydrophobicity or alkyl chain length and by ligand density or stoichiometry of substitution. By thus controlling the degree of hydrophobicity, adsorption to alkyl agaroses can be tuned to show differences in adsorption that might otherwise be too subtle to detect.

Solution depletion was chosen as a technique for monitoring

protein concentration changes due to adsorption. This method is amenable to high-surface-area materials such as hydrophobic alkyl agaroses.

Protein molecules, having both hydrophobic and hydrophilic surface sites, adsorb to strongly hydrophobic surfaces, primarily through hydrophobic bonding and to highly hydrophilic surfaces, predominantly through polar and donor-acceptor interactions, although on many surfaces both mechanisms play major roles. After initial adsorption or close apposition of surface and protein, the protein molecule may change its conformation and/or orientation. More compliant surfaces may also exhibit some accommodation, thus increasing adsorption affinity.

Alkyl groups on an agarose substrate have some mobility in solution, enabling limited movement. This ability permits many conformations of the attaching ligand to the protein molecule in addition to the possiblity of ligand self aggregation. Tha alkyl group may fold on itself; it may then be unfolded by the protein during the adsorption process if the protein is in close proximity for a sufficient time period.

Adsorption would likely be a stepwise procedure to include (Fig. 1):

1. Transport to the surface site;
2. Initial secondary bonding interaction and attachment;
3. Alignment of strongest adsorption sites;
4. Propagation of segmental attachment;
5. Optimal alignment of adsorptive interactions;
6. Possible conformation changes, probably coupled with Step 5.

The process from Step 2 to Step 3 would determine if adsorption will occur. Depending upon affinity and the relative time course, desorption could occur at any time. The equilibria set up will be combinations of metastable states, not easily determinable.

1. Solution transport

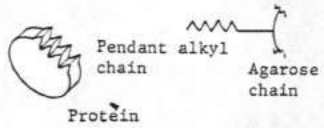

2. Initial secondary bonding interaction

3. Alignment of the strongest adsorption sites

4. Propagation of segmental attachment

5. Optimal alignment of strongest sites

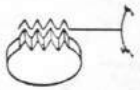

6. Steric strain, conformational accommodation

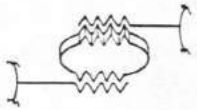

Figure 1. Protein adsorption schemata.

Hemoglobin

Normal hemoglobin (HbA, which will be the only Hb considered) contains two pairs of unlike polypeptide chains whose sequences are well known (14-18). Each chain contains one heme group in a pocket of nonpolar amino acid residues near the surface of the protein. A heme is a prosthetic group consisting of an iron atom surrounded by a prophyrin ring. The four chains are in a rough tetrahedral arrangement with the resulting molecule approximately spherical. The two different polypeptide chains have been called α and β chains so that the full molecule is indicated as $\alpha_2\beta_2$. Of the 141 amino acids in the α chain, and 146 in the β chain, more than 75% are in an α-helical conformation. The helical segments are designated by letters A to H, residues of each helix are then numbered. Interdigitating areas carry the two-letter designation of adjacent helices. This system provides continuity in following terminilogy of α and β chains and the residues are thence readily comparable.

The interior of the tetramer contains primarily nonpolar residues, while polar residues occur on the surface of the tetramer and in a central cavity, which contains water.

The various parts of the Hb tetramer, the four chains and the four heme groups, are <u>not</u> bound by covalent bonds. The protein must be considered in a state of reversible equilibrium with its components. Dissociation to dimers and monomers is favored by several factors including high or low pH, high electrolyte concentration, etc. that may be "native" to the Hb molecule.

The packing of Hb chains is such that there is close interlocking

and contact between unlike chains, but very minor communication between like chains. Contacts between dissimilar chains are primarily hydrophobic in nature ($\alpha_1\beta_2$, $\alpha_1\beta_1$), while contacts between like subunits are due to ionic interactions ($\alpha_1\beta_2$, $\alpha_1\beta_2$).

The $\alpha_1\beta_1$ contact is more extenisve than the $\alpha_1\beta_2$ type (6), and it would be expected that the dimer of choice would be $\alpha_1\beta_1$, although the significance of this point is unknown. Upon dimerization, one would expect that additional hydrophobic surfaces would be exposed to the aqueous milieu; however, the Hb dimer solution conformation is not well documented (5,6). If there is any reaccommodation of αβ chains in the dimer, the hydrophobic patchwork so well known in the tetramer becomes subject to interpretation.

Protein structure is a dynamic phenomenon with random thermal fluctuations, Brownian motion, electrolyte diffusion, etc. The protein molecule must <u>not</u> be considered a rigid sphere capable of exhibiting a constant surface structure, e.g. hydrophobic clefts may show transient appearance.

Tetrameric oxygenated and deoxygenated Hb have very different solution conformations. Upon deoxygenation, the β chains move away from each other and out from the center of the tetramer. The distance between the iron atoms in the β chains increase on deoxygenation. Deoxy- and ligand-bound Hb (where the ligand can be O_2, CO_2, NO, and others) differ in other properties which may be sutides in solution, including (19,20).

Side group reactivity, Affinity and rates of reaction with small molecules, rates of digestion by proteolytic enzymes, antibody

reactions are different for oxy- and deoxy-Hb (19), reaction with Hp, and association-dissociation into subunits.

Dissociation constants for oxy-Hb and deoxy-Hb are approximately $2*10^{-6}$ and $1*10^{-12}$, respectively (20). The concentration ranges where dimers and tetramers are present in equal concentration are 0.032 mg/ml and $1.6*10^{-8}$ mg/ml, respectively, for oxy-Hb and deoxy-Hb.

Deoxy-Hb is a tight structure, stabilized by salt bridges between the amino and carboxyl groups on the respective terminal ends of each polypeptide; other internal salt bridges also exist. These salt bridges are successively broken during reaction with ligands. Sequential rupture of salt bridges during oxygenation leads to alterations in the tertiary and quaternary structures. Oxygenated Hb is a more relaxed structure by virtue of losing several constraining salt bridges.

In addition to salt bridges, the presence of organic phosphates leads to decreased oxygen affinity by Hb. Intracellular concentration of 2,3 diphosphoglycerate (2,3 DPG) appears to be one of the major controls of the oxygen affinity of Hb. The binding site of 2,3 DPG appears to be on the β chains in the central cavity of the deoxygenated tetramer. Bound 2,3 DPG is not found in the oxygenated form, rather it is extruded out from the central cavity when the Hb undergoes conformational changes upon ligand binding, during which additional salt bridges must be severed. The effects of binding of 2,3 DPG appear to be increased stabilization of the deoxy form (and decreased oxygen affinity).

The relation between the state of aggregation of Hb and ligand equilibrium may be considered from two points of view: the effect of

dissociation into subunits on the oxygen equilibrium, and the effect of oxygenation on the association-dissociation equilibria (21,22). There are contradicting data in the literature (17,18,22), as to the functional unit in Hb being either dimeric or tetrameric. Certainly both α and β chains must be present. The question of dimerization of deoxy-Hb is not well defined.

Deoxyhemoglobin is more stabilized and hence more likely to exist in tetrameric form than oxy-Hb in conditions favoring dimerization of oxy-Hb.

Knowing the minute concentration of Hb in plasma, it would be expected that circulating free Hb would be in dimer form if hemolysis occurred on the arterial side, i.e. in the oxy form, whereas, if hemolysis occurred on the venous side, free Hb would be in the tetrameric deoxy form, stabilized by salt bridges and internally bound 2,3 DPG.

The Hp is known to bind oxy-Hb and deoxy only if dimerization can indeed take place (23). Deoxyhemoglobin is not bound in a reasonable physiologic time frame; however, it must be noted that even when the Hp-Hb complex is deoxygenated, the binding is <u>not</u> reversed.

Normal Hb exists in ferrous form (Fe^{++}) but can undergo autooxidation to the ferric form (Fe^{+++}). The ferric form can bind ligands as NO^-, OH^-, CN^-, etc.; however, heme-heme interactions, the Bohr effect and others are lacking in the reactions of ferric Hb with ligands. The conformation of the ferric liganded forms is very similar to oxy-Hb. Only the deoxy-Hb tetrameric solution conformation differs in quaternary structure from all other forms of tetrameric Hb. Cyano-liganded ferric Hb is extremely stable and is the most commonly used Hb when degradative procedures may compromise the protein integrity.

The various forms of Hb are summarized in Figure 2.

Media Effects

Secondary, tertiary, and quaternary protein strucutres are dictated by intramolecular interactions with the solvent media, including other solutes. The conformation is very sensitive, generally, to environmental influences such as pH, ionic strength, etc., because one conformation may be only marginally more thermodynamically favored. Contributing interactions are mainly coulombic, hydrogen bonding, and hydrophobic.

Alkyl Agaroses

In the native biological conformation, proteins are folded in part to minimize exposed hydrophobic side chains. However, proteins have hydrophobic patches on their surface, which are presented to the aqueous environment. The hydrophobic groups exposed are not limited to relatively small ones, but include some larger side chains as phenylalanine and tryptophan (24). Hydrophobicity appears to be a general characteristic of proteins and probably plays an important role in the recognition process in vivo.

The study of hydrophobic bond formation with large hydrophobic groups is hampered by the relatively low solubility of such compounds. Highly hydrophobic and insoluble compounds can be "solvated" with an agarose vehicle by covalent linkage of a hydrophobic ligand to an insoluble but hydrophilic matrix.

A sufficiently large hydrophobic patch on the protein interface may constitute a binding site for the hydrocarbon chains bound onto the relatively inert agarose. The relative flexibility of the bonded

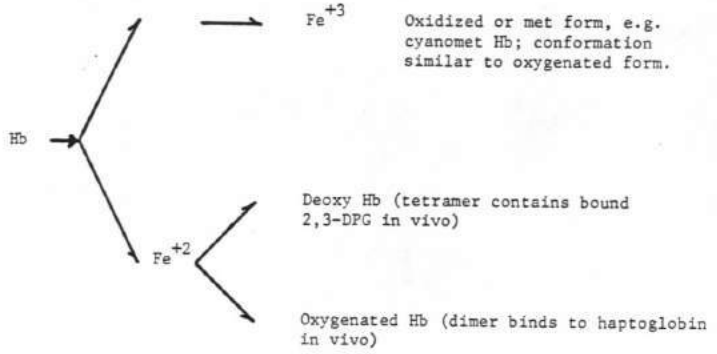

Figure 2. The various forms of hemoglobin (Hb).

hydrocarbon chain affords the possibility of accessing protein hydrophobic pockets and accommodating the surface hydrophobic patches in whatever manner is most energetically favorable. It is assumed that the available hydrophobic patches on the protein surface vary in size, shape, lipophilicity and surface density, and that these variations are manifest in the relative affinities of the protein for the agarose alkyl ligands, to be discussed later.

Most alkyl agaroses are prepared by cyanogen bromide (CNBr) activation of the agarose followed by alkyl coupling via an amino alkyl compound. The secondary amino group probably retains its basic property and is at least partially positively charged at physiologic pH. The shorter amino alkanes may display electrostatic contributions (25-28); although Halperia, et al. (25) have shown that protein interactions with alkyl agaroses are almost totally due to hydrophobic interactions.

The alkyl group on the agarose matrix is believed to exist adjacent to the aqueous interface on a heterogenous or homogenous planer lattice of binding sites. The agarose matrix is freely penetrable to Hb. However, an excessive alkyl substitution may lead to self aggregation of the butyl or octyl groups, and subsequent collapse of the agarose matrix. It is possible that the substituted agarose alkyl groups do self associate, to some degree, and thus protein adsorption may be partially a competition process.

Protein binding is a function of both ligand density and alkyl chain length (hydrophobicity) (25,26,28). In hydrophobic chromatography, where alkyl agaroses see primary usage, the hydrophobicity of

the agarose gel serves as the discriminator for protein purification. It is found that as the hydrophobicity of the gel is increased, higher binding forces result and desorption of proteins is usually accomplished via salt gradients, to selectively desorb competing species. Elution of proteins from a hydrophobic matrix parallels salting-in phenomena, as desorption is dependent on the type of salt employed and not on the ionic strength, per se (26,29).

It is postulated that protein adsorption or retention may be stepwise. Jennisen hypothesizes (30) hydrophobic nucleation and propagation, whereas Milchek (27) advocates coulombic initiation with subsequent hydrophobic synergistic interactions (the relative merits of these respective ideas will not be discussed but are presented as insight into the myriad of possibilities). Jennisen has inferred from Scatchard and Hill plots a critical hydrophobicity for nucleation (31).

MATERIALS AND METHODS

Hemoglobin

Bovine red cells, freshly collected, were sedimented from citrated blood by centrifugation, and washed five times in 0.15 M sodium chloride (NaCl). The buffy coat was aspirated with each wash. Packed, washed red cells were lysed in 10 volumes of distilled deionized water. The ghosts were sedimented by centrifugation at 30,000 G for 20 minutes at 4° C. After adjustment of the pH to 6.8 as necessary, the supernatant was applied to a carboxymethyl-cellulose column (CM52, Whatman) previously equilibrated with 5 mM potassium phosphate buffer (pH 6.8) until the effluent was colorless. The adsorbed Hb was eluted with 1.0 M potassium phospahte (pH 6.8). The eluate was extensively dialyzed against 0.15 M Na-saturated PBS (pH 7.4) and placed in a pure N_2 atmosphere for 30 minutes to deoxygenate the Hb. The source was then stored at 4° C under nitrogen.

Oxygenated Hb (HbO_2) was obtained by aerating, by exposure to atmosphere for 10 minutes the deoxy-Hb. It was never stored as HbO_2.

Cyanomet Hb was prepared by reacting Hb in an excess of $K_2Fe(CN)_6$ and NaCN and then dialyzing extensively against 0.15 M PBS (pH 7.4).

Alkyl Agaroses

Two chain lengths of alkyl agarose were employed, butyl and

octyl. Synthesis involves two processes, activation of the parent agarose by CNBr, and coupling of the alkyl chain. The method of Kumel, et al. (32) was used to activate and the method of Shaltiel (33) to couple.

The method of Kumel features reaction control of the CNBr activation by slow transit of CNBr from a dispersed organic phase, to the aqueous phase containing agarose beads in concentrated buffer. CNBr was dissolved in the original flask by adding 0.5 ml acetonitrile per gram CNBr, yielding a final concentration of 1 g/ml. Agarose (Sepharose 4B from Pharmacia) aliquots of 15.0 ml of settled gel were washed three times on a filter funnel, sucked dry with an aspirator, and added to 225 ml 3.3 M potassium phosphate (dibasic) with pH adjusted to 11.5 via KOH (at a ten-fold dilution), and placed in 2-liter Erlynmeyer flasks on magnetic stirrers. To control the degree of activation the stoichiometry of CNBr was adjusted; the CNBr added was 25, 50, 100, and 150 mg CNBr/ml dry sucked agarose, respectively, at each of the aliquots. The reaction was stirred vigorously for 10 minutes with crushed ice added to stop the reaction. The agarose slurry was placed in a filter funnel and washed with 1.5 liters of ice-cold, distilled water, sucked dry and added to 300 ml of 0.1 M $NaHCO_3$ (pH 9.5).

The n-alkyl amine (4 moles per mole of CNBr used for activation) was dissolved into 4 volumes of a solution containing equal volumes of N,N-dimethyl formamide (DMF) and 0.1 M $NaHCO_3$. The alkylamine-DMF-$NaHCO_3$ was added to each aliquot of activated agarose and the reaction stirred at room temperature for 20 hours.

The agarose slurries were washed with 5 volumes of each of the following: a) water, b) 0.2 M acetic acid (CH_3COOH), c) water, d) 50 mM NaOH, e) water, f) dioxane-water (1:1), and g) 0.2 M CH_3COOH: Then washed with 20 volumes of water. Finally, each solution was washed and equilibrated with 0.15 M PBS (pH 7.4) and pH adjusted if necessary. As a control, CNBr activated (150 mg CNBr/ml dry, sucked gel) agarose was coupled with ammonia as above. This allowed any adsorption attributed to nonhydrophobic means or artifacts of the adsorption process to be detected.

Alkyl substitution levels were determined via an NMR technique developed during the course of this experimentation (38).

Adsorption Experiments

Precautions had to be taken when handling oxygenated or deoxygenated Hb. In preparing either of these, the solutions must be handled in pure 0_2 or N_2 atmospheres, respectively. This requires equilibration of solutions prior to handling, and all solution preparation, dispensing, etc., must be performed in a glove box until the culture tubes are anaerobically capped (see below). Solutions of cyanomet-Hb can be handled in atmospheric conditions.

For adsorpiton studies on the alkyl agaroses, either butyl or octyl, protein solutions were simultaneously mixed for the entire series, including a calibration standard and an ammonia-coupled agarose control; a known volume (3 to 4 ml) was placed in culture tubes. Alkyl agarose slurries were equilibrated with N_2 (or 0_2 in $Hb0_2$ solutions) to facilitate $C0_2$ removal. One milliliter of alkyl agarose

slurry for each of the series was placed in the protein solution culture tubes, sealed, and incubated in a shaker bath at 37° C for 48 hours. Calibration standards for each protein solution concentration were subjected to identical conditions, except that no glass or agarose was added. Adsorbed protein was taken to be the change in concentration between each calibration tube and its respective adsorption sample.

All samples were centrifuged for 15 minutes at 1500 relative centrifugal force (RCF) and the supernatant decanted off for protein concentration determinations. Concentrations were monitored spectrophotometrically on a Perkin-Elmer Hitachi UV-VIS spectrophotometer. Extinction coefficients were taken from the literature for all proteins (5). However, a visible absorption spectrum was run on a Cary spectrophotometer to check the HbO_2 and deoxygenated Hb spectra for extinction maxima and to detect any major spectral shifts due to ferric Hb formation during the course of incubation.

The inability in determining deoxygenated Hb concentration aerobically after incubation required deoxy-Hb conversion to HbO_2, accomplished by gentle swirling in an open culture tube for 10 minutes prior to measurement. Extinction coefficients for HbO_2 were then used.

RESULTS

The results of protein adsorption experiments must be carefully and cautiously examined. If adsorption isotherms fit certain forms described by classical theory, the adsorption behavior itself is sometimes interpreted via the same theory. Should the attendant premises of the theory hold, the analysis can be made in a straightforward manner. However, for the purposes of this study, which is only an initial feasibility investigation of the adsorption behavior of Hb on alkyl agaroses, a rigorous analysis is neither necessary nor appropriate.

Data are presented as adsorption isotherms with the amount of protein adsorbed, micrograms (µg) of protein per micromole (µM) alkyl ligand, plotted against the final protein solution concentration in mg/ml. Two concentration regions are plotted. The first includes protein concentration up to 1.5 mg/ml and is intended to show broad adsorption isotherm characteristics (Figs. 3 through 6). The second is an expanded scale which covers the protein concentration range only up to 0.10 mg/ml, which indicates adsorption behavior at low concentrations (Figs. 7 through 10). Figures 3 through 10, A through D, indicate increasing alkyl ligand density ranging as follows:

A = 8.8 µM alkyl ligand per gram of dry sucked gel.

B = 10.8 µM alkyl ligand per gram of dry sucked gel.

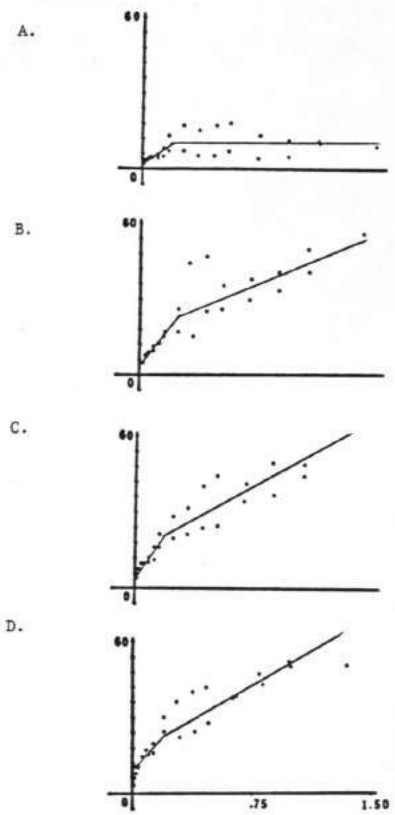

Figure 3. Cyanohemoglobin adsorption on octyl agarose.

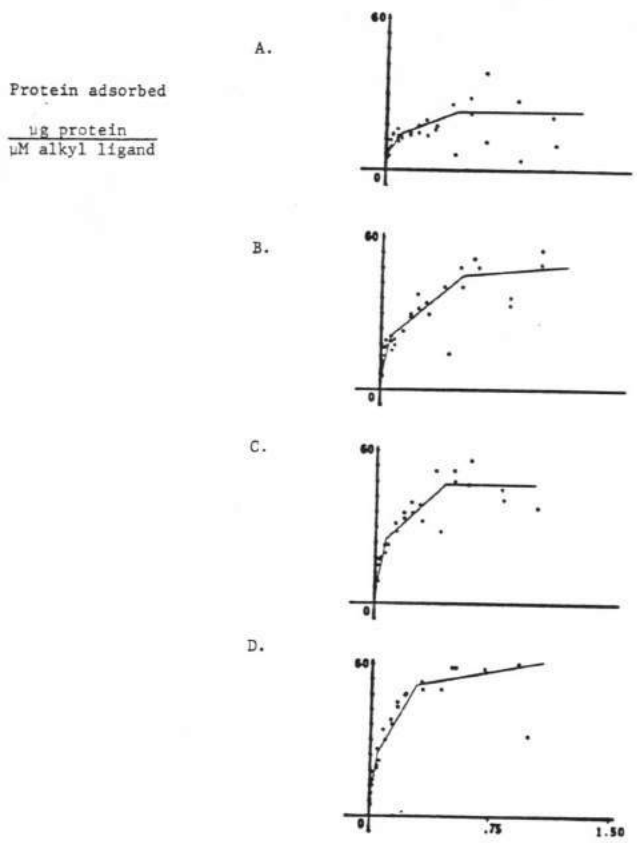

Figure 4. Oxygenated hemoglobin adsorption on octyl agarose.

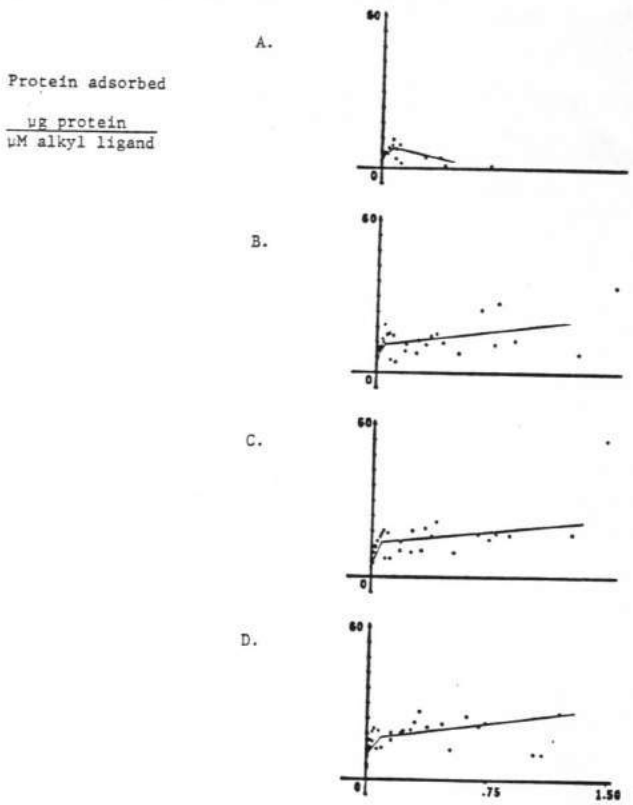

Figure 5. Deoxygenated hemoglobin adsorption on octyl agarose.

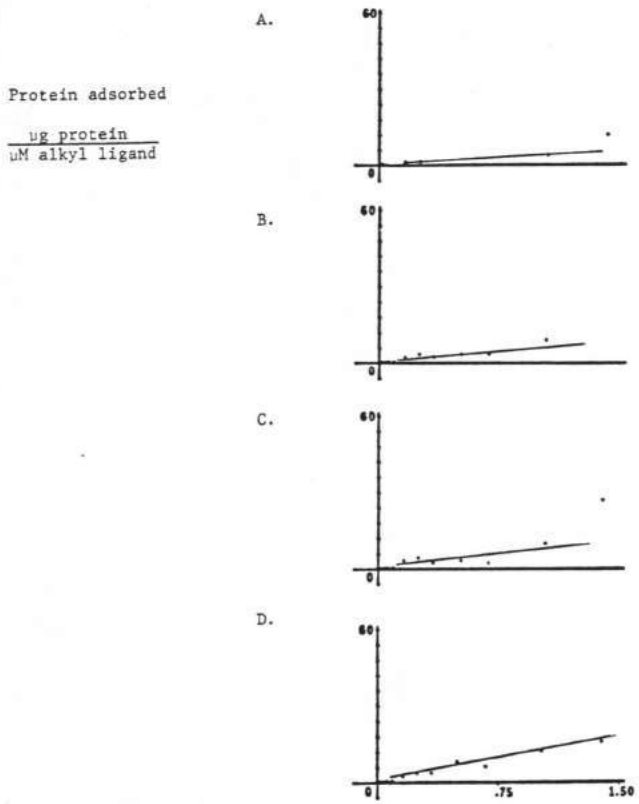

Figure 6. Cyanoglobin adsorption on octyl agarose.

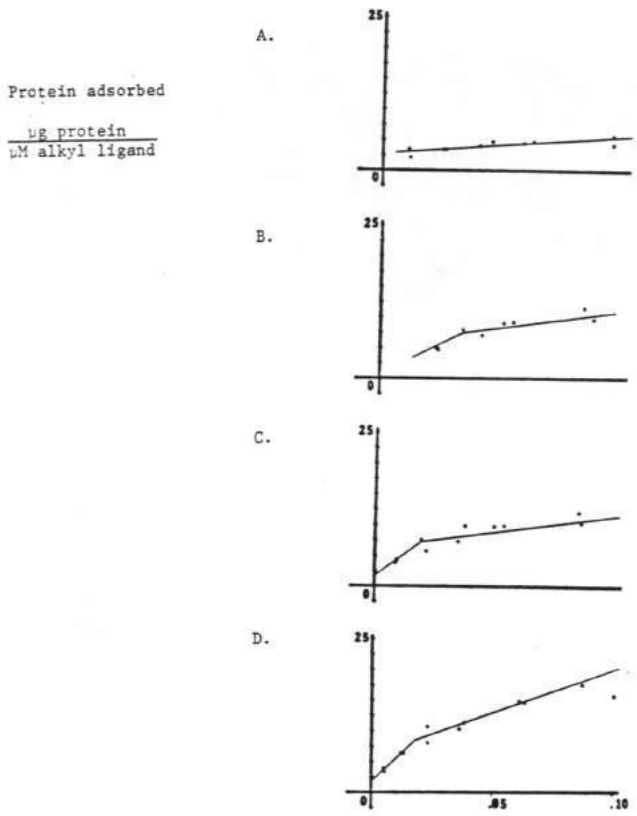

Figure 7. Low solution concentration adsorption of cyanohemoglobin on octyl agaroses.

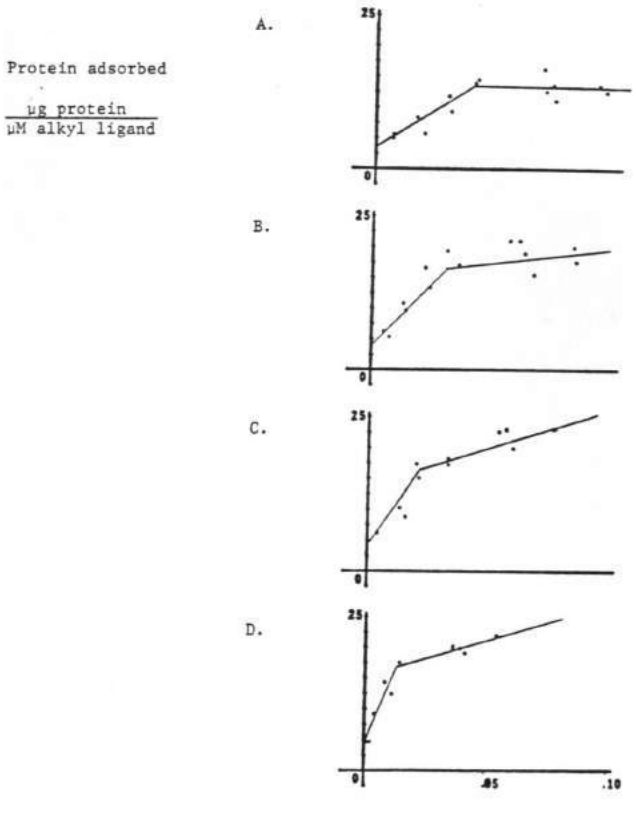

Figure 8. Low solution concentration adsorption of oxygenated hemoglobin on octyl agaroses.

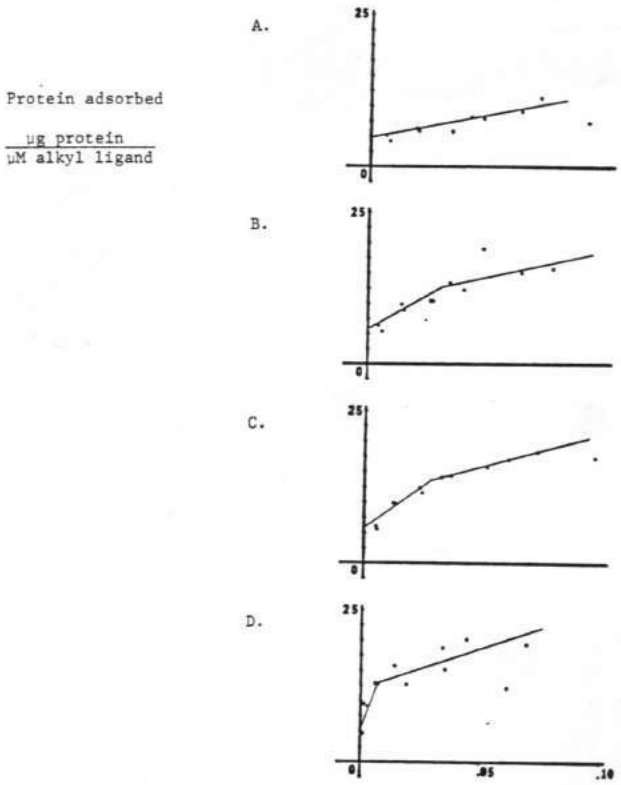

Figure 9. Low solution concentration adsorption of deoxygenated [illegible]globin on octyl agaroses.

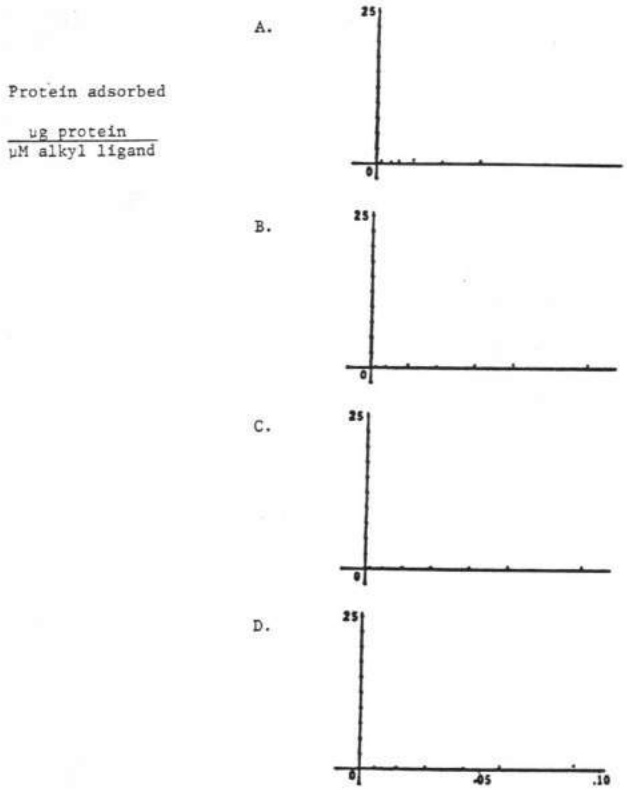

Figure 10. Low solution concentration adsorption of cyanoglobin on octyl agaroses.

C = 11.4 μM alkyl ligand per gram of dry sucked gel.

D = 17.4 μM alkyl ligand per gram of dry sucked gel.

These correspond directly to the four CNBr levels used in the agarose activation procedure (refer to Materials and Methods, Alkyl Agaroses).

The minimum Hb concentration changes necessary for detection at the lowest concentration regions, in the solute depletion method used in this study, were approximately 0.002 mg/ml. This corresponds to interface adsorption levels on the order of 1.0 μg protein adsorbed per μM alkyl ligand. As the concentration is increased in following the isotherm, the concentration changes for detectability increase accordingly. The concentration changes monitored during repeated adsorption experiments of Hb on butyl agarose in this experimental series were far less than the detectable limits. It was concluded that little or no adsorption occurred for Hb on butyl agarose.

Examine first the difference in adsorption behavior of the different alkyl densities in the low concentration regions (Figs. 7 through 10). As the ligand density increases from top to bottom in the figures (A through D), the protein adsorption increases for deoxy-Hb, HbO_2, and HbCN as evidenced by both magnitude of adsorption and the affinity (related to isotherm slope). The slope increases in successively higher liganded series in each case, with roughly similar incremental increases noted in all three liganded hemoglobins, although the adsorption behavior of the three are different.

The adsorption of HbCN has an initial shallow slope and low level of adsorption in Figure 7a, and shows no plateau or break in the isotherm. In Figure 7b the initial level is low but the slope has increased slightly and no plateau or break is seen. Figure 7c has a higher initial slope but has a break point and a lower slope thereon. Figure 7d parallels Figure 7c, but both initial and following slopes are higher and the break point moves to a lower solution concentration. Both Figures 7c and 7d show Langmuir-like forms.

The behavior of deoxy-Hb (Fig. 9) is similar to HbCN, with a stronger initial slope increasing through Figure 9c. However, by Figure 9d, the initial affinity has increased dramatically and the break in the isotherm is both more pronounced and displaced to a lower concentration.

The HbO_2 has the highest initial slope starting in Figure 8a, and a Langmuir-like form. Proceeding down through Figure 8, the slope increases and the break in the isotherm is likewise displaced to a lower final solution concentration. Cyanoglobin (Fig. 10) has very little adsorption in this initial concentration region.

At the higher concentration regions (Figs. 3 through 6), the adsorption differences become more discernible. The HbCN, in Figure 3a, rises to a plateau value at a low solution concentration. In Figure 3b and 3c, the behavior is similar with approximately the same adsorbed values reached at corresponding solution concentration levels. The adsorption affinities increase slightly in proceeding through increasing ligand densities, Figure 3a

through Figure 3d. Only the first break point is displaced to a lower solution concentration at higher alkyl ligand densities.

The HbO_2 displays different adsorption behavior. The initial slope in Figure 4a is greater than for HbCN, and at the break point where HbCN plateaus, adsorbed HbO_2 continues to increase, although with no further break points noticed. Proceeding through Figure 4b through 4d, the curves roughly parallel the behavior of HbCN with a greater slope in each respective series. However, the break points move to lower solution concentrations in going from Figure 4b to Figure 4d.

Deoxyhemoglobin displays completely different behavior in this concentration region. Both the slope and the adsorbed levels attained by Hb isotherms differ from HbCN and HbO_2. The initial slope does not increase as drastically as do those for HbCN and HbO_2, dependent upon ligand density. The protein adsorbed at higher solution concentration values does change with ligand density, but not as much as might be expected. Beyond an initial break point in the isotherms, the protein solution concentration does not appear to exert much effect, except in Figure 5a.

Cyanoglobin adsorbs in a constantly increasing manner, with no plateau observed. The slope increases with increasing ligand density, as seen from Figure 6a to Figure 6d.

DISCUSSION

Hemoglobin exists in solution form in a dynamic equilibrium between tetrameric and dimeric forms. In the concentration ranges used in this study, the predominant equilibrium shifts from dimer to tetramer, with increasing solution concentration for both HbCN and HbO_2 (refer to Hemoglobin under Background). Deoxyhemoglobin is normally a tetramer and does not dimerize until far lower concentrations ($< 1*10^{-6}$ mg/ml).

The Hb association-dissociation equilibria is influenced by the local microenvironment and may be affected by the presence of agarose and alkyl units. Kinetic recombination and diffusion would be inhibited, as would the probability of adsorption of dimeric species. Thus, the concentration at which dimerization occurs in the vicinity of a surface will be less well defined and probably broadened over previously determined ranges.

Dimerization adds numerous possibilities to the mechanism of adsorption. The fresh surface area formed upon dimerization probably has a greater preponderance of hydrophobic bonding sites. Adsorption thus becomes a competition process between dimers and agarose alkyl residues. If binding is reversible, the adsorption reversibility may involve displacement of a protein molecule by another exchange process, or by desorption alone. Displacement may occur if a tetramer is displaced from an adsorption site by a dimer for more energetic

bonding. If a tetramer dissociates to dimer form upon adsorption due to steric strain, kinetics, etc., another possibility becomes competition with bound dimers competing for solvated dimers.

Kinetics play an important role in adsorption, e.g. the rates of arrival, equilibration, structural accommodation, desorption, etc. Reversibility, with respect to dilution, is usually employed to sort out desorption kinetics. However, the fact that Hb undergoes changes in dimer-tetramer equilibria with changes in concentration, suggests that reversibility with regards to dilution will be a very difficult experiment to interpret.

Rates of arrival for the differing species would be expected to be different, as would the orientations of the arriving protein molecules. Brownian motion and diffusion are providing movement to the protein molecules and limited displacements to the agarose helices and alkyl substituents. A descriptive look at the adsorption process becomes necessary before suggesting conclusions.

Figure 11 is a sketch of the possibilities for interaction between Hb and alkyl agaroses, grouped into three categories:

1. Ongoing competitive binding that definitely affect adsorption levels and affinities.

2. Possible ongoing competitive binding that affect binding to a far lesser degree.

3. Possible hindrances to binding originating from the alkyl group's hydrophobic preference of minimizing water contact area.

As a protein approaches a binding site, a logical progression arises to facilitate adsorption:

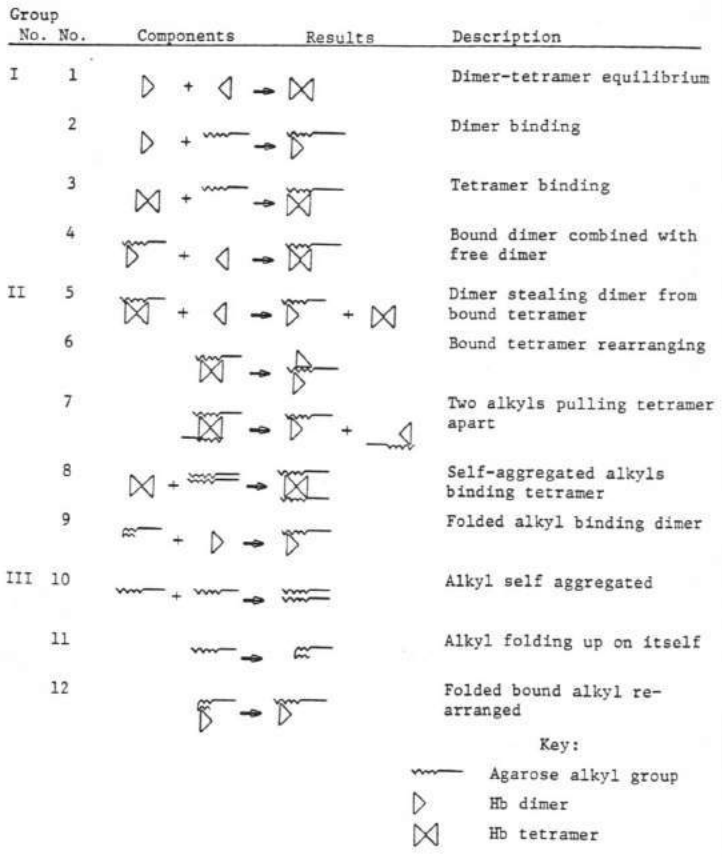

Figure 11. Competitive adsorption processes.

1) Transport of the protein molecule and access to the site;
2) Stoppage or slowing down of motion relative to protein and binding site;
3) Ample residence time to ensure necessary secondary bonding interactions;
4) Alignment of most energetically favorable secondary bonding sites;
5) Propagation of segmental attachment;
6) Synergism of adsorption attractions such as ion pair facilitation by hydrophobic environments through dielectric media effects (34);
7) Surface accommodation by protein and/or adsorbent, thus maximizing number and affinity of site interactions;
8) Steric strain may pull the protein into a nonnative form, which is less likely to be resolvated with sufficient strength to desorb.

Disruption of the binding may occur for many reasons:

1) The protein kinetic energy may be too great for retention, or may statistically contribute to a short residence time.
2) A nonsufficient bonding strength for propagation or synergistic action leading to metastable states (35).
3) More favorable binding by time-dependent changes and accommodation by the agarose substrate.

With the complex competitive processes during adsorption and

the different alkyl residue environments, it is best not to emphasize binding affinity constants nor Hill coefficients at this time. The adsorption affinity constant will change as saturation of preferential sites occurs. Although binding can be considered on a planar lattice of uniformly distributed sites (30), this is probably not the case to the extent of extracting a discrete set of binding constants from Scatchard data (35).

The adsorption behavior is indeed an involved and complicated process. A few salient details should be considered herein. The HbO_2 may undergo auto-oxidation during the experimental time course. To guard against this, extreme precaution was used in equilibrating all components in the experiment with O_2 prior to experimentation. Nonetheless, some HbO_2 would be expected to convert to the ferric form during the experiment and hence become very much like HbCN regarding conformation and solution properties. The problem with the ferric form in HbO_2 is the obscuring of data by preferential adsorption of either form, and thus confounding data interpretation. However, it is seen from the data that HbCN and HbO_2 do indeed act quite differently.

Deoxy-hemoglobin is much more stable against auto-oxidation, and would not be expected to degrade to the ferric form nearly as readily as HbO_2. Again, it is seen that deoxy-Hb acts quite differently than does HbCN.

The adsorption increases observed when using progressively higher alkyl substituted agaroses may stem from geometric implications. The contact sites accessible to each molecule (in solution

form, dimer-tetramer) are more numerous, leading to greater strength of attraction. Ion-pair facilitation, mediated by dielectric media changes, becomes more favorable.

The break points on the isotherm, moving to lower solution concentrations as higher alkyl ligand densities are employed, are at approximately constant levels of protein adsorption, i.e. the level of adsorption is invariant at the break point, even as the adsorption affinities change. The break point adsorption level appears to be characteristic of the particular liganded Hb, in the concentration range being examined. The affinity of adsorption appears to be mediated by a combination of Hb type and alkyl ligand density.

The following arguments may be major contributors to the adsorption behavior of differently liganded hemoglobins.

1. The tetrameric solution conformation of deoxy-Hb, HbCN, and HbO_2 are all very similar without significant difference to positively ascribe any differences in binding capabilities. The most probable differing contribution will be the ferric form (HbCN), which has lost the ability for heterotropic interaction (Bohr effect), where the acid-base interaction with the aqueous milieu and alkyl attachment environment is lost. This consideration would add to the interaction ability of HbO_2 and deoxy-Hb with the partially basic character of the secondary amine of the alkyl-agarose coupling (over and above that of HbCN).

2. Dimer-tetramer equilibria of the various hemoglobins is very much different. The dissociation constant of HbO_2 is much greater (10^{-6}) than that of deoxy-Hb (10^{-12}) and roughly equal to

HbCN. With the exposed hydrophobic contacts (6) available in the dimer form, dimer binding to the alkyl agarose would be both more frequent and more tenacious. At extremely low solution concentrations, initial binding by this means of deoxy-Hb, HbCN, and HbO_2, will be similar. As the concentration is increased, deoxy-Hb will demonstrate the lesser affinity, as the dimerized proportion drops much more rapidly than HbO_2 or HbCN (refer to Appendix).

This may partially explain the anomalous behavior of deoxy-Hb adsorbing to the lowest alkyl density agarose as higher concentrations are approached. Possibly the preponderance of dimers that have formed have not had enough time to encounter an alkyl group before combining with another dimer. Competitive adsorption would be skewed towards dimer-dimer interaction and away from alkyl-ligand-dimer interaction at this weaker alkyl residue density.

CONCLUSIONS

The differently liganded hemoglobins HbCN, HbO_2, and deoxy-Hb indeed show different adsorption characteristics to alkyl agaroses. At concentrations comparable to those which may exist in vivo under conditions of localized hemolysis, HbO_2 and deoxy-Hb show differences in adsorption on artificial surfaces that may indicate preferential adsorption possibilities in the circulatory system.

Adsorption isotherm break points occur at approximately constant levels of adsorption and seem to be a characteristic of the particular liganded Hb in the concentration range being examined. The affinity of adsorption appears to be mediated by a combination of Hb type and alkyl ligand density.

These studies were performed with pure solutions. The results of similar studies were performed in plasma would probably be very different. A more complete description of isotherm behavior could be recorded that would then enable more rigorous data analysis to be performed (35).

More advanced techniques are now available to monitor real time adsorption behavior. One such method is total internal reflection fluorescence spectroscopy (TIRF) (36). This method would enable differentation in real time of adsorption behavior of differently liganded hemoglobins, to be monitored in situ directly.

ACKNOWLEDGEMENTS

This work was partially supported by NIH Grants HL18519 and HL .

REFERENCES

1. Horbett, T. A., Weathersby, P. K., and Hoffman, A. S., Journal of Bioengineering 1, 61-77 (1977).

2. Horbett, T. A., Weathersby, P. K., Hoffman, A. S., Thrombosis Research 12, 319 (1978).

3. Horbett, T. A., Journal of Biomedical Biomaterials Research 15, 673 (1981).

4. Genkin, M. V., Biofizika 23, 796, (1978); Chemical Abstracts 90, 1959q (1979).

5. Benko, B., Davydov, R. M., and Krylov, O. B., Journal of Colloid and Interface Science 52, 44 (1975).

6. Pommerening, K., Vukpavlos, S., Dezelic, G., and Maricic, S., Journal of Polymer Science Symposium 68, 79 (1980).

7. Hirsch, R. E., Ristau, O., Jung, W., Kuhn, M., Mohr, P., and Scheler, W., Journal of Colloid and Interface Science 78, 212 (1980).

8. Memoli, V. A., and Doellgast, G. J., Biochemical and Biophysical Research Communications 66, 1011 (1975).

9. Chukhrai, E. S., Veselova, M., Poltorak, O. M., and Pryakhin, A. N., Chemical Abstracts 86, 166619j (1977).

10. Hallaway, B. E., Hallaway, P. E., Tisel, W. A., and Rosenberg, A., Biochemical and Biophysical Research Communications 86, 689 (1979).

11. Brietenback, M., in "Affinity Chromatography" (O. Hoffman-Ostenhof, M. Breitenbach, F. Koller, D. Kraft, and D. O. Scheiner, Eds.), p. 175, Pergamon, London, 1978.

12. Dvorankova B. and Pavlicek, Z., Collection of Czechoslovak Chemical Communications 46, 1288 (1981).

13. Gendreau, R. M., Leininger, R. I., Brown, L. L., Winters, S., Jakobsen, R. J., "FT-IR of Whole Blood-Polymer Interactions" submitted to ASAIO Journal.

14. Cooper, R. A., in "Hematology" (Williams, W. J., Beutler, E., Erslev, A. J., and Rundles, R. W., Eds.) 2nd Ed., pp. 216-229. McGraw Hill, New York, 1977.

15. Nagel, R. L., and Gibson, Q. H., The Journal of Biological Chemistry 246, 69-73 (1971).

16. White, P., "Hematology" (Williams, W. J., Beutler, E., Ersler, A. J., and Rundles, R. W., Eds.) 2nd Ed., pp. 230-236. McGraw Hill, New York, 1977.

17. Antonini, E., and Brunori, M., "Hemoglobin and Myoglobin in Their Reactions with Ligands" North Holland Publishing Co., Amsterdam, 1971.

18. Dickerson, R. E., and Geis, I., "The Structure and Action of Proteins", pp. 44-59, Harper and Row, New York, 1979.

19. Antonini, E., Science 158, 1417-1425 (1967).

20. Thomas, J. O. and Edelstein, S. J. Journal of Biological Chemistry 247, 7870-7874 (1972).

21. Ranney, H. M. "Hematology" (W. J. Williams, E. Beutler, A. J. Ersler, and R. W. Rundles, Eds.) 2nd Ed., pp. 196-202. McGraw Hill, New York, 1977.

22. Antonini, E., and Chiancone, E., Annual Review of Biophysics and Bioengineering 6, 239-271 (1977).

23. Nagel, R. L., Personal Communication, March 1980.

24. Klotz, I. M., Archives of Biochemistry and Biophysics 138, 704-706 (1970).

25. Halperin, G., Breintenback, M., Tauber-Finkelstein, M., Shaltiel, S., Journal of Chromatography, in press.

26. Hofstee, B. H. J., Journal of Macromolecular Science--Chemistry A10, 111-147 (1976).

27. Wilchek, M., and Miron, T., Biochemical and Biophysical Research Communications 72, 108-113 (1976).

28. Jennissen, H. P., Journal of Chromatography 159, 71-83 (1978).

29. Jennissen, H. P., Biochemistry 14, 754-760 (1975).

30. Jennissen, H. P., Protides Biological Fluids 27, 765-770 (1979).

31. Jennissen, H. P., Botzet, G., International Journal of Biological Macromolecules 1, 171-179 (1979).

32. Kumel, G., Daus, H., Mauch, H., Journal of Chromatography 172, 221-226 (1979).

33. Shaltiel, S., Methods Enzymology 34, 126-140 (1974).

34. Warshel, A., Proceedings of National Academy of Science U.S.A. 75, 5250-5254 (1978).

35. Jennissen, H. P., "Affinity Chromatography and Molecular Interactions" (Jean M. Egly, Ed.) pp. 253-264 INSERM, Paris, 1979.

36. Van Wagenen, R. A., Rockhold, S. and Andrade, J. D., "Morphology, Structure and Interactions of Biomaterials" (S. L. Cooper, A. S. Hoffman, N. A. Peppas, B. D. Ratner, Eds.) American Chemical Society, 1982, in press.

37. Rosengren, I., Pahlman, S., Glad, M., and Hjerten, S, Biochem. Biophys. Acta, 412, 51 (1975).

in "Sol-Gel Science & Technology", E.J.A.Pope, S. Sakka, and L.C.Klein,eds.(American Ceramic Society, Westerville, OH, 1995).

Pope
(18)

LIVING CERAMICS

E. J. A. Pope*
Matech Advanced Materials,
31304 Via Colinas, Ste. 102, Westlake Village, CA 91362.

K. Braun, M. Van Hirtum, C. M. Peterson
Sansum Medical Research Foundation,
2219 Bath St. Santa Barbara, CA 93105.

P. Tresco and J. D. Andrade
Dept. of Bioengineering, University of Utah,
2480 Merrill Engineering Bldg., Salt Lake City, UT 84112

ABSTRACT

Various live microorganisms and mammalian tissue cells can be encapsulated in porous inorganic gels for such possible applications as sensors, pharmaceutical bioreactors, and artificial internal organs. For example, *saccharomyces cerevisiae* has been encapsulated in a transparent matrix of porous, gel-derived silica. After gelation, aging, and prolonged storage at 5°C, *S. cerevisiae* bioactivity could be triggered. Bioactivity was followed by evolution of alcohol within the *S. cerevisiae* as a function of time during incubation by the molecular probe molecule pyranine using fluorescence spectrophotometry. In addition, mammalian tissue cells, such as pancreatic islet cells, adrenal cells, and hepatocytes, have all been encapsulated into silica gels. Encapsulated mouse islets have been transplanted into diabetic mice with success. Described also are other potential applications of this new class of biocomposite material incorporating a "living" second phase.

*to whom correspondances should be addressed.

INTRODUCTION

In this report, living microorganisms and mammalian tissue cells have been incorporated into a transparent, porous silica gel matrix while preserving their bioactivity. Because the cells are approximately three orders of magnitude larger than the average pore diameter of the gel matrix, they are effectively immobilized. The fine porosity of the gel, however, permits nutrients to reach the living cells and byproducts to escape. It may be possible to encapsulate many other microorganisms and tissue cells in a similar manner.

The sol-gel route enables the preparation of a wide range of porous, inorganic solids from liquid solutions at temperatures near ambient (1,2). Porous silica gels possessing high transparency can be prepared from alkoxide-based solutions with porosities as low as only a few percent to as high as 99 percent (3).

In recent years, numerous research groups have demonstrated the successful incorporation of a wide range of organic molecules into gel-derived materials, including microstructural probes (4,5), laser dyes(6-9), nonlinear optic dyes (6,10), enzymes (11), and microorganism-derived molecules(12). The nanometer level porosity of the gel-derived host allows the encapsulated dopant to be both chemically and optically accessible(13). The immobilization of yeast spores and certain bacteria in silica has been demonstrated (14-21).

S. cerevisiae has been the subject of recent studies into the fundamental nature of various proteins on cellular processes (22) and the genetic processes occuring during meiosis(23-28). Other microorganisms, such as genetically modified *E. Coli* and *Streptomyces* bacteria, have emerged as highly promising "factories" for a wide range of therapeutic enzymes(29). Genetically engineered *Pseudomonas putida* has been demonstrated to metabolize polyhalogenated compounds, such as pentachloroethane and tetrachloroethane, into environmentally-friendly by-products(30). It has been recently observed that plasmid

DNA in bacteria manifest liquid crystal mesophases which exhibit significant optical polarization effects (31).

The microencapsulation of living cells, not microorgansisms, such as Islets of Langerhans, hepatocytes, and parathyroid cells "have the potential to be used clinically for the treatment of diabetes, hepatic failure, and parathyroid insufficiency, respectively (32)". The separation of the cells from the immune system of the patient by a semi-permeable membrane, in the case of islets, permits the free migration of glucose and insulin while excluding direct contact with antibodies (33). These are a few examples of possible scientific, medical, and technological benefits of this novel class of materials.

S. CEREVISIAE

The encapsulation of a living microorganism, *saccharomyces cerevisiae*, in porous, transparent silica gel, in which the bioactivity of the organism is preserved, is presented. The bioactivity has been studied by staining the *S. cerevisiae* with a molecular probe, pyranine.

Saccharomyces cerevisiae is a single cell ascomycete fungi(34). Used in the fermentation of beers and whiskeys, and the raising of breads, it is one of the oldest cultured plants or organisms by man. The chief result of its bioactivity is the conversion of sugars and carbohydrates to ethyl alcohol and CO_2. Hence, bioactivity can be followed by measurement of ethanol produced. 8-hydroxy-1,3,6-trisulfonated pyrene trisodium salt, henceforth refered to as pyranine, has been demonstrated as an excellent molecular probe for water content of reverse micelles(35,36), pH changes in phospholipid vesicles(37,38), and the study of the chemical evolution of aluminosilicate sols and gels (39,40). Pyranine can exist in both a protonated, PyOH, and deprotonated, PyO^-, form, depending upon either pH or water content of solution. The protonated form exhibits a strong blue luminescence at ~430 nm, while the deprotonated form fluoresces at ~515 nm(40). The relative ratio of alcohol to water, for example, can be easily

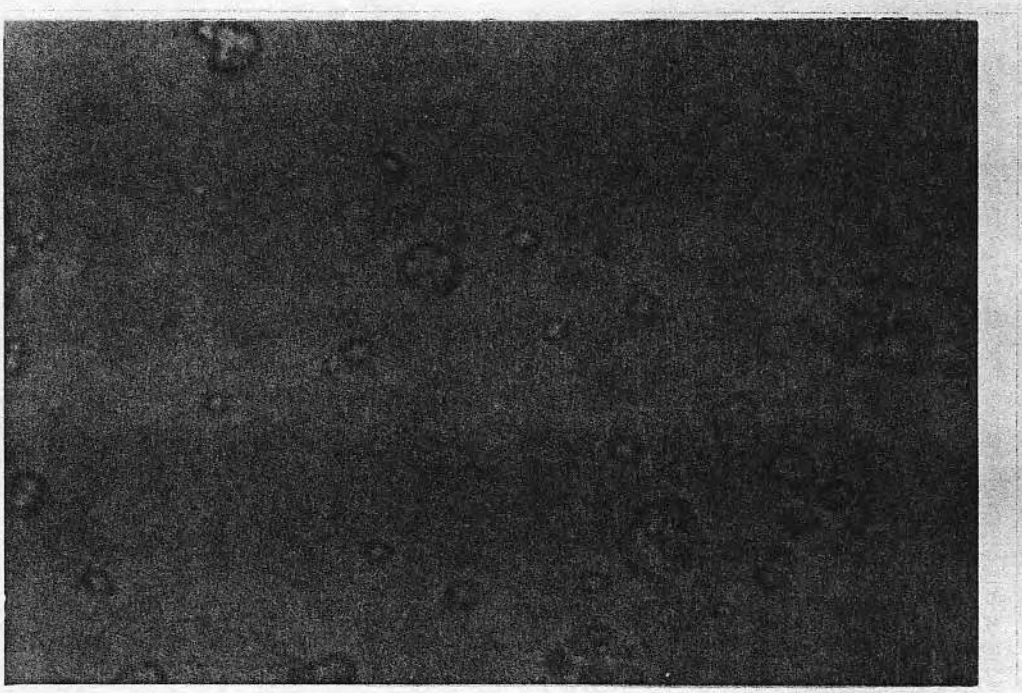

Fig. 1: Photomicrograph (400X) of pyranine-stained saccharomyces cerevisiae on a glass microscope slide. Individual saccharomyces appear to be approximately 10.0 microns in length and 8.0 microns in width.

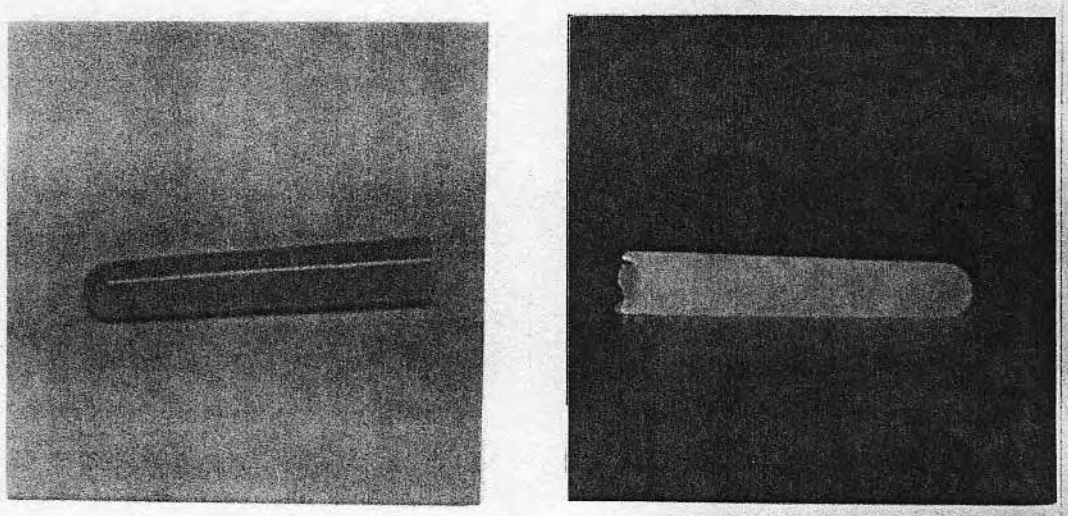

Fig. 2: Photograph of silica gel encapsulated, pyanine-stained S. cerevisiae biocomposite: A) under incandescent light; B) under UV (365 nm) illumination. Sample length approximately 7.0 cm, diameter approximately 1.0 cm.

followed by measureing the relative ratio of PyOH to PyO^- fluorescence (40). Pyranine was selected for this study as a molecular probe to document *S. cerevisiae* bioactivity.

Prior to usage, *S. cerevisiae* was stained by pyranine in the following manner. 0.5 gm *S. cerevisiae* (SIGMA Chemical Company) was dispersed in 20 cc distilled water by gentle mixing, after which 2.0 cc of pyranine (Eastman Fine Chemicals) solution (1×10^{-3} M in distilled water) was added. The stained *S. cerevisiae* can then be stored for future use or used directly. A photomicrograph of stained *S. cerevisiae* on a microscope slide is presented in figure 1. The dye molecule is readily absorbed by the fungus.

Due to the pH sensitivity of *S. cerevisiae* silica gels were prepared by the two-step method of Brinker (41), in which hydrolysis of the silicon alkoxide precursor is achieved under acidic conditions and gelation is induced through the addition of base. Tetraethoxysilane (TEOS), purchased from Morton Thiokol, Alfa Products, 42.0 cc, was vigorously mixed with 10.0 cc 0.1 M HCl solution. After 30 minutes of stirring, the initially turbid mixture became a clear solution due to the hydrolysis of TEOS and the associated evolution of ethanol. The solution was then chilled in an ice bath to reduce the rate of polycondensation upon the addition of base. 15.0 cc 0.1 M ammonium hydroxide solution was rapidly added. After one minute of stirring, 20.0 cc of prestained *S. cerevisiae* dispersion was introduced and the gel forming solution was cast in capped polyethylene test tubes. Gelation occured within a few minutes. The pH immediately prior to gelation was measured to be approximately 5.0. The gels were then stored at 5°C. A photograph of the resulting silica gels doped with stained *S. cerevisiae* is presented in figure 2. The gels appear biege under normal room light and fluoresce bright green under 365 nm UV illumination. In figure 3, a photomicrograph of a small gel fragment is presented under both transmission and UV illumination. The gel is transparent except for the individual and clustered *S. cerevisiae*. The average pore diameter of the silica gel phase was calculated to be 10.0 nm, based upon surface area and porosity measurements (42).

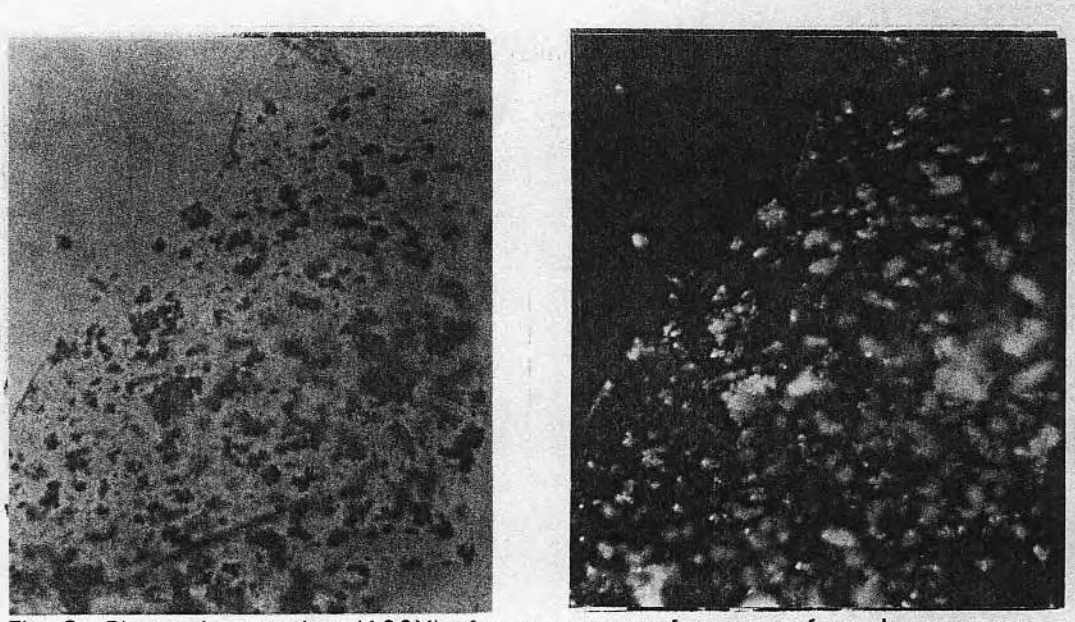

Fig. 3: Photomicrographes (100X) of a transparent fragment of saccharomyces encapsulated in silica gel: A) under transmitted light; B) under UV (365 nm) side illumination. Individual and clustered saccharomyces cerevisiae are the dark spots in (A) and the bright spots in (B).

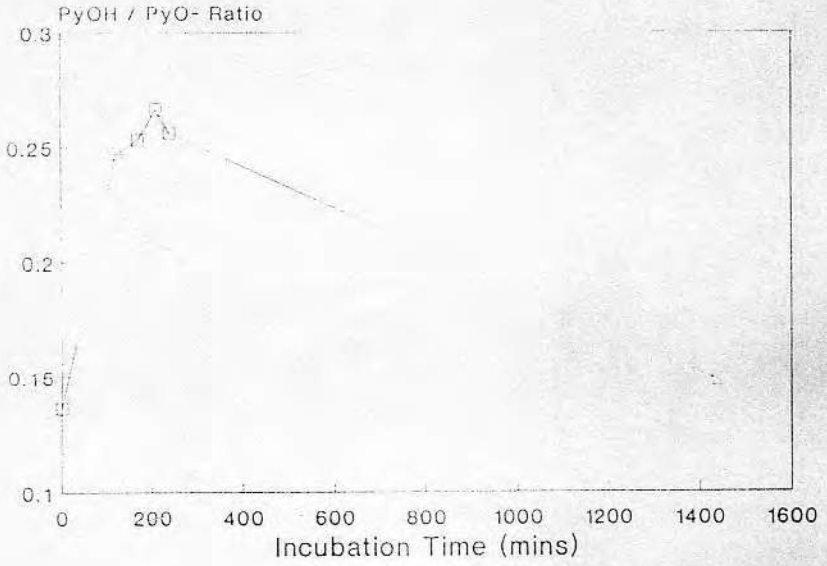

Fig. 4: Ratio of the protonated to deprotonated fluorescence peaks of pyranine vs. incubation time at 45oC for free S. cerevisiae in a formula of galactomannan polysaccharides, sucrose, and water.

In order to promote fermentation, a food formula consisting of 25 gm of galactomannan polysaccharides (SIGMA Chemical Co.), 50 gm of sugar, mixed with 1000 cc. of distilled water was prepared, henceforth refered to as "food formula". An initial test of the bioactivity of the *S. cerevisiae* was preformed. 30.0 cc. of food formula was mixed with 20.0 cc of prestained *S. cerevisiae* emulsion and incubated at 45°C in a sealed glass sample vial. In figure 4, the ratio of the fluorescence peaks of protonated to deprotonated pyranine is plotted vs. incubation time. The bioactivity of the *S. cerevisiae* peaks at approximately 200 minutes after incubation was initiated, indicating the production of ethanol within the fungus. Fermentation was also confirmed by the formation of "foam" at the top of the sample vial, a pressure build-up inside the vial, and the appearance of a strong oder commonly associated with fermentation processes. As the biological activity of the fungus decreases, the concentration of ethanol byproduct within the bacteria declines due to diffusion into the surrounding liquid. In figure 5, the fluorescence spectra of pyranine stained *S. cerevisiae* is presented. Curve "A" is the fluorescence emission spectrum prior to incubation and curve "B" is the spectrum at the peak of bioactivity. Prior to incubation, only a small shoulder corresponding to the protonated pyranine is present. As ethanol is produced within the *S. cerevisiae*, a much stronger peak at about 443 nm appears. By plotting the ratio of the intensities of $PyOH/PyO^-$ vs. volume percent ethanol in aqueous solutions, the peak alcohol concentration within the *S. cerevisiae* was estimated to be approximately 40 volume percent.

In order to test for the bioactivity of the *S. cerevisiae* -doped silica gels, gel samples were solvent exchanged in distilled water twice for 24 hours at 5°C to remove residual alcohol produced during the initial hydrolysis. The washed gels were then impregnated with food formula containing galactomannan polysacharides, sugar, and water for 24 hours at 5°C. Prior to incubation, the gel samples were removed from the food furmula solution and quicky rinsed in distilled water to remove surface deposits of food formula and any stray *S. cerevisiae*. The fully impregnated gel samples were then incubated

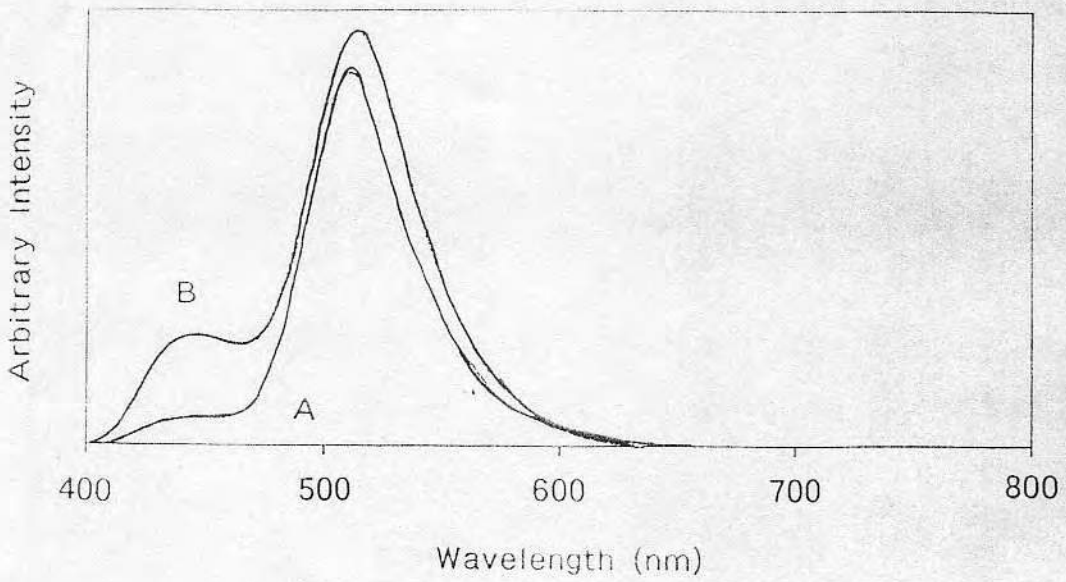

Fig. 5: Fluorescence spectra of pyranine-stained saccharomyces cerevisiae from figure 4 at: A) 0 minutes incubation time; B) 200 minutes incubation time.

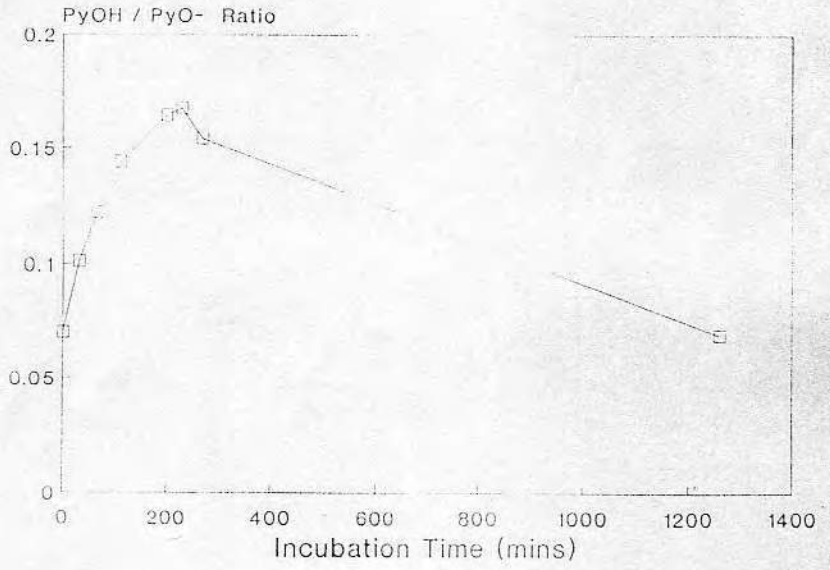

Fig. 6: Ratio of the protonated to deprotonated fluorescence peaks of pyranine vs. incubation time at 45°C for silica gel encapsulated S. cerevisiae impregnated with a formula of galactomannan polysaccharides, sucrose, and water.

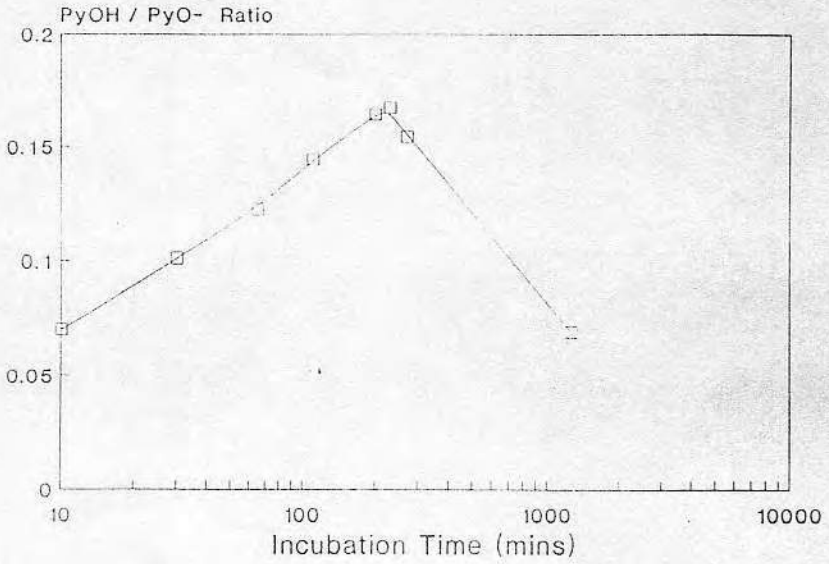

Fig. 7: Ratio of the protonated to deprotonated fluorescence peaks of pyranine vs. logarithm of incubation time at 45oC for silica gel encapsulated S. cerevisiae impregnated with a formula of galactomannan polysaccharides, sucrose, and water.

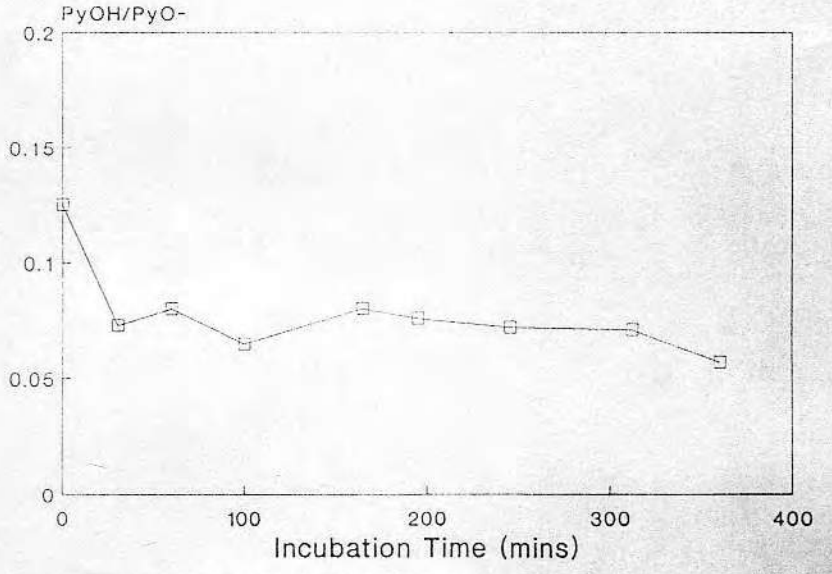

Fig. 8: Second cycle ratio of the protonated to deprotonated fluorescence peaks of pyranine vs. incubation time at 45°C for silica gel encapsulated S. cerevisiae impregnated with a formula of galactomannan polysaccharides, sucrose, and water.

in a sealed glass vial at 45°C and the emission spectra measured at various time intervals. A plot of the ratio of $PyOH/PyO^-$ as a function of incubation time is presented in figure 6, following a pattern similar to that of free *S. cerevisiae* shown in figure 4. The peak bioactivity also occurs at approximately 200 minutes after incubation was initiated. The peak alcohol content within the gel-encapsulated *S. cerevisiae* was calculated to be approximate 30 volume percent, about 10 volume percent less than in the case of free *S. cerevisiae*. In figure 7, the $PyOH/PyO^-$ ratio is plotted vs. the logarithm of incubation time, showing a logarithmic rise and fall in ethanol content within the *S. cerevisiae.* To the unaided eye, there was no observable change of appearance of the gel samples. There was, however, a pungent oder produced by the fermentation, similar to that observed for the case of free *S. cerevisiae.*

To determine if the observed bioactivity could be repeated, or cycled, by the same samples, the samples described above were "reprocessed" by solvent exchange in water twice for 24 hours, to remove fermentation byproducts, and then impregnated for 24 hours with fresh food formula. Samples were then incubated at 45°C and spectra measured at various time intervals. In figure 8, the second cycle bioactivity is plotted vs incubation time. No significant change over time was observed, suggesting that bioactivity in this system could not be sustained for repeat cycles. The causal mechanism of the inhibition in second cycle bioactivity is the subject of further study.

BOVINE HEPATOCYTES

In order to investigate the morphological consequences of encapsulating mammalian tissue cells, fresh bovine hepatocyte tissue (beef liver) was enzymatically dispersed by the method of Quistorff, Dich, and Grunnet (43), using an enzymatic solution of 60 mg. collagenase and 60 mg. dispase in 120 mL Hank's Balanced Salt Solution (HBSS) under gentle agitation at 37°C for 2 hours. The resulting supernatent of isolated hepatocytes was decanted and used for encapsulation. Similar to the method described above, 20 cc. hepatocytes solution was added to the silica solution prior to

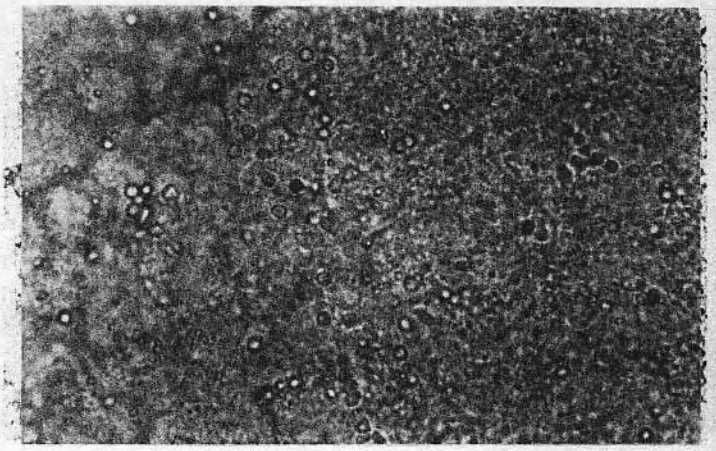

Fig. 9: Photomicrograph of bovine hepatocytes encapsulated in porous silica gel (400X).

Table 1: Insulin secretory response following sol-gel encapsulation.

Source	Time Post Encapsulation	FSR/hour*
Control fetal pancreas	1 week	3.63
Control adult islets	1 week	1.43
C57 Bl fetal pancreas,	1 week	1.55
		2.14
		1.2
C57 Bl adult islets	1 week	1.46
		1.58
		1.62
C57 Bl fetal pancreas	3 weeks	1.75
		4.36
		2.7
C57 Bl adult islets	3 weeks	0.27
		1.45
		4.38
		3.36
Control fetal pancreas	3 weeks	0.29**
Control adult islets	3 weeks	0.4**

*fractional stimulatory ratio

**loss due to infection

gelation. In figure 9, isolated bovine hepatocytes encapsulated in silica gel is shown at X100 magnification. The majority of cells appear round and their structure is well-preserved. No test of bioactivity was performed on these cells, inasmuch as they were not live tissue cells.

MOUSE ISLETS

Working in collaboration with the Sansum Medical Research Foundation, pancreatic cells, islets of Langerhans, have been encapsulated in porous silica gel. In figure 10, a typical mouse islet culture is shown. Unlike the hepatocytes, islets are obtained from surgically removed whole pancreas and minced into sub-millimeter cell clusters. Fetal mouse islets and adult mouse islets encapsulated in silica gel produced insulin in response to glucose challenge. In table 1, preliminary insulin secretory response data are presented for control cultures and encapsulated cultures of both adult and fetal mouse islets *in vitro*. After 3 weeks, both fetal and adult islets performed well to glucose challenge, while control cultures performed poorly due to infection. Silica gel encapsulation may have prevented bacterial overgrowth.

Transplantation of encapsulated islets into a diabetic mouse was recently performed. The diabetic mouse strain (see figure 11) at Sansum has been designated Smrf by the National Research Council Institute of Laboratory Animal Resources. After one month of transplantation, the surgically removed transplant showed no evidence of fibrosis. Further *in vivo* transplant studies are in progress. Life span *in vivo* and host/implanted tissue immunologic and/or fibrotic responses are currently under investigation. Transplanted islets of Langerhans, if viable for extended lengths of time, could emerge as a viable treatment for diabetes(44).

RAT PC-12 CELLS

At the Department of Bioengineering, University of Utah, an aggressive research program, under the direction of Dr. Pat Tresco, is underway to develop encapsulated cells for sustained neurotransmitter delivery to the central nervous system(45).

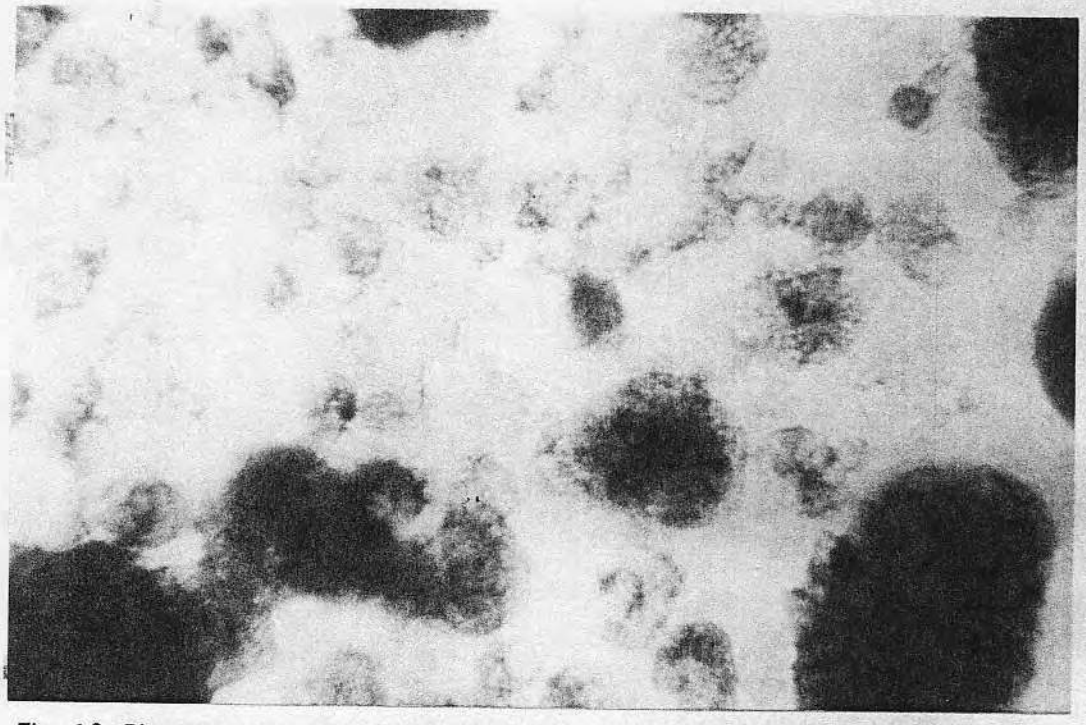

Fig. 10: Photomicrograph of a typical culture of minced fetal islets. Largest clusters are approximately 1.0 mm in diameter (C.M. Peterson, et al., "Human fetal pancreas transplants", J. Diabetic Complications, 3 (1989) 27-34.

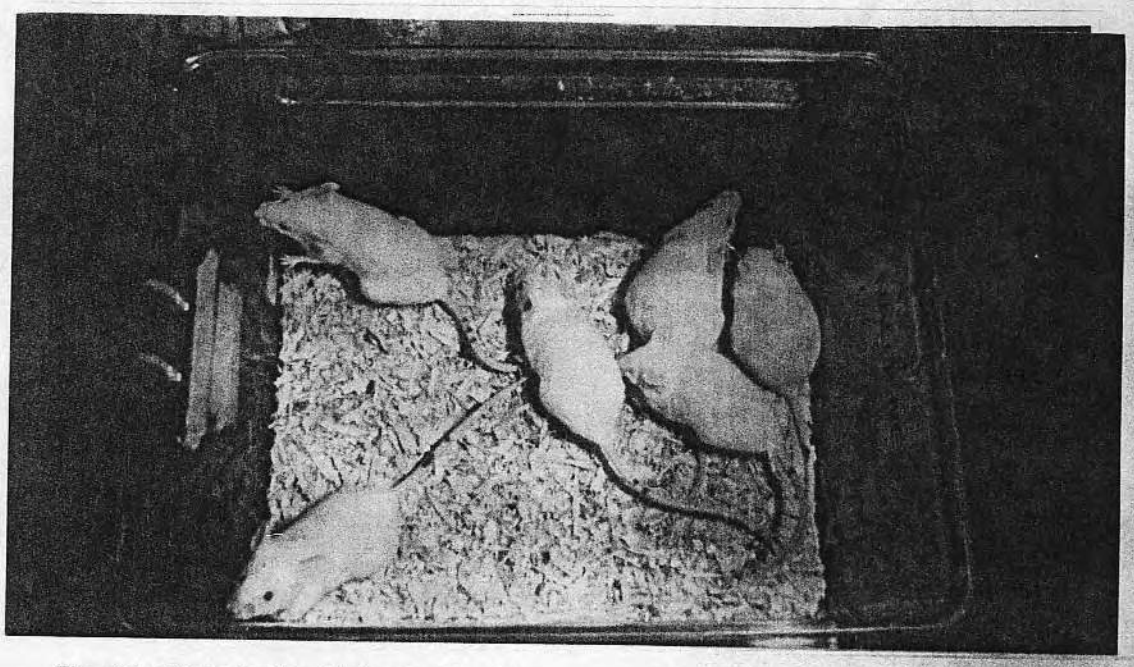

Fig. 11: Diabetic Smrf laboratory mice.

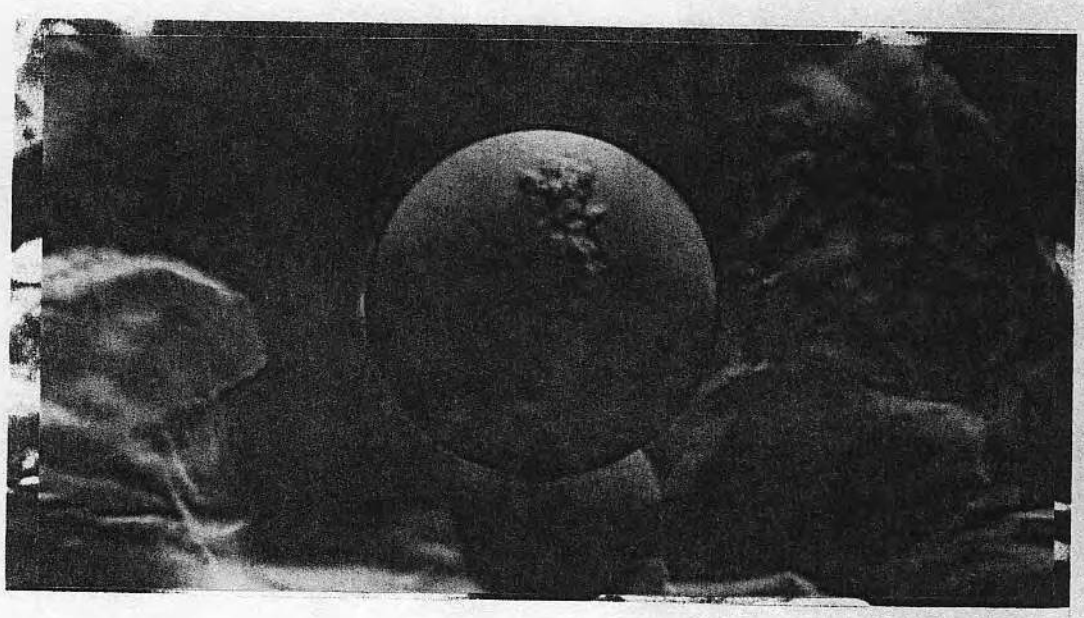

Fig. 12: Photomicrograph of rat PC 12 adrenal cells encapsulated in a silica gel spheroid.

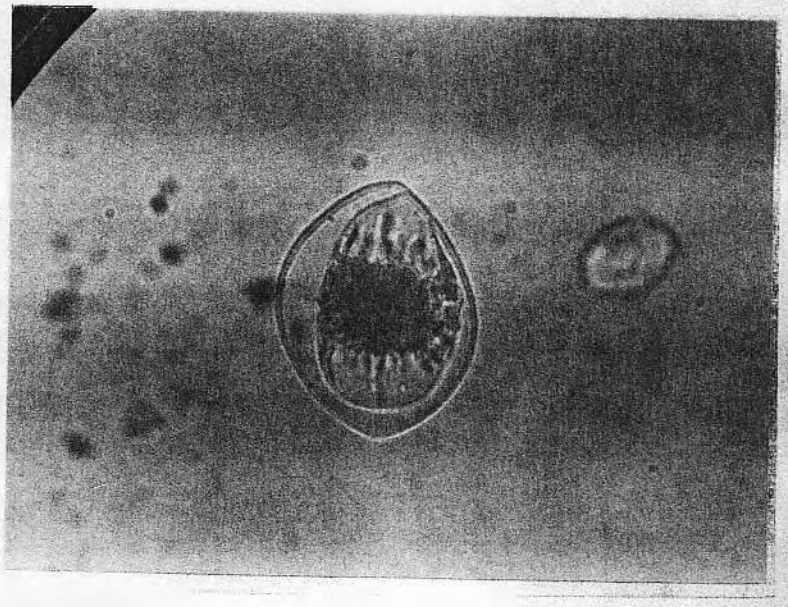

Fig. 13: Photomicrograph (X100) of an individual *P. lunula* encapsulated in silica gel.

Implantable, bioartificial prosthesis may find therapeutic usefulness in treating central nervous system disorders, such as Parkinson's disease (45). PC 12 cells, isolated from rat pheochromocytoma, were dispersed in silica gel spheroids, based upon the solution chemistry described for *S. cerevisiae* (20,21). Upon gelation, samples were immersed in growth media and incubated at 37°C under 5% carbon dioxide. A photomicrograph of the dispersed PC 12 containing spheroid is shown in figure 12. Preliminary tests with vital dye staining indicate cell viability after encapsulation. Further tests to determine dopamine secretory response are in progress.

BIOLUMINESCENT MICROORGANISMS

The bioluminescent species of dinoflagellate, *Pyrocystis lunula*, is a photosynthetic algae which live within the top 100 feet or so of most of the earth's oceans(46). At night, upon agitation, such as wave action or the movement of fish, they luminesce bright blue. It has been speculated that this luminescence is related to predator aversion. *P. lunula* (Protein Solutions, Inc., Salt Lake City, Utah) were encapsulated in the same manner as *S. cerevisiae*, except that all solutions used in gel hydrolysis and formation contained 2.9 % NaCl by weight. In figure 13, a silica gel encapsulated *P. lunula* is shown. Thus far, however, no bioluminescence in encapsulated dinoflagellates has been observed. This does not necessarily indicate a lack of bioactivity. The "trigger" for the bioluminescence is agitation. Confined within a rigid silica matrix, it may be impossible to induce bioluminescence. Ultrasonic vibration, sample fracture, and other means of creating shock waves within the material have, thus far, all failed to achieve detectable luminescence. Current efforts are directed towards bioluminescent bacteria.

SUMMARY

In this report, living microorganisms, such as *Saccharomyces cerevisiae* and *Pyrocystis lunula*, have been incorporated into a transparent, porous silica gel matrix while preserving their

bioactivity. Mammalian tissue, such as mouse islets of Langerhans and rat PC 12 adrenal cells, have also been encapsulated. Preliminary results suggest that long term immunoisolation and pathoisolation for the transplantation of cells is promising. Because the cells are approximately three orders of magnitude larger than the average pore diameter of the gel matrix, they are effectively immobilized. The fine porosity of the gel, however, permits nutrients to reach the cells and byproducts to escape. It may also be possible to encapsulate a wide range of other microorganisms and mammalian tissue cells in a similar manner for scientific study, medical and industrial applications. The encapsulation of pancreatic islets, adrenal cells, and hepatocytes for transplantation into animal hosts appears promising for bioartificial organs.

REFERENCES

1. J. D. Mackenzie, *J. Non-Cryst. Sol.*, **48**,1(1982).
2. B. I. Lee and E. J. A. Pope, eds., "Chemical Processing of Ceramics", (Marcel-Dekker, New York, 1994).
3. E. J. A. Pope and J. D. Mackenzie, *J. Non-Cryst. Sol.*, **87**,185(1986).
4. D. Avnir, D. Levy, R. Reisfeld, *J. Phys. Chem.*,**88**,5956(1984).
5. T. Tani, H. Namikawa, K. Arai, A. Makashima,*J. Appl. Phys.*, **58**, 3559(1985).
6. E. J. A. Pope, J. D. Mackenzie, *MRS Bull*, **12**[3],29(1987).
7. E. T. Knobbe, B. Dunn, P. D. Fuqua, F. Nishida, *Appl. Optics*,**29**[18],2729(1990).
8. B. Dunn, et al, in *Better Ceramics Through Chemistry III*, MRS Symp. Proc. **121**, 331(1988).
9. E. J. A. Pope, *J. Sol-Gel Sci. & Tech*, **2**, 717(1994).
10. T. Che, et al, *J. Non-Cryst. Sol.*,**102**, 280(1988)
11. S. Braun, et al, *Mater. Lett.*, 10, 1 (1990);L. M. Ellerby, et al, *Science*, **255**, 1113(1992); S. A. Yamanaka, et al, *Chem. Mater.*4[3], 495(1992).
12. S. Wu, et al, *Chem. Mater.*,**5**[1],115(1993).
13. P. Lucan, et al, in *Sol-Gel Optics II*, SPIE Symp. Proc. Vol. **1758**, 464(1992).
14. G. Carturan, et al, *J. Mol. Catal.* **57**, L13 (1989)
15. S. Braun, et al. *Biotechnology:Bridging Research and Applications*, Kamley, et al, eds.(Kluwer, Netherlands, 1991)205-218.
16. M. Uo, et al, *J. Ceram. Soc. Japan*, **100**[4], 426 (1992)
17. L. Inama, et al, *J. Biotech.*, **30**, 197(1993)
18. J. Livage, et al, in *Sol-Gel Optics III*, J. D. Mackenzie, ed (SPIE Symp. Proc. Vol. **2288**, 1994)493-503.
19. D. Avnir, et al., *Chem. Mater.*, **6**(1994)1605-1614.

20. E. J. A. Pope, "Gel Encapsulated Microorganisms: S. cerevisiae-silica biocomposites", presented at the Pacific Coast Regional Meeting of the American Ceramic Society, Los Angeles (October 19-22, 1994).
21. E. J. A. Pope, *J. Sol-Gel Sci. & Tech.*,(1995) in press.
22. Y. Ohya and D. Botstein, *Science,* **263**, 963(1994).
23. R. H. Morse, *Science*, **262**, 1563(1993)
24. T-C. Wu and M. Lichten, *Science*,**263**,515(1994).
25. T. Maeda, et al, *Nature*, **369**, 242(1994).
26. R. B. Wickner, *Science*, **264**, 566 (1994).
27. M. Foss, et al.,*Science*, **262**, 1838 (1993).
28. H. Liu, C. A. Styles, and G. R. Fink, *Science*, **262**, 1741(1993).
29. R. McDaniel, et al, *Science*, **262**, 1546(1993).
30. L. P. Wackett, et al. *Nature*, **368**, 627 (1994).
31. Z. Reich, J. Wachtel, and A. Minsky, *Science*, **264**, 1460(1994).
32. A. M. Sun, et al, in "Artificial Organs", J. D. Andrade, et al, eds. (VCH Publishers, New York:1987) 613.
33. C. K. Colton and N. L. Weinless, in "Artificial Organs", J. D. Andrade, et al, eds. (VCH Publishers, New York:1987) 641.
34. G. W. Burns, *The Science of Genetics: An Introduction to Heredity*, in *The Molecular Biology of the Yeast Saccharomyces: Metabolism and Gene Expression*, J. N. Strathem, E. W. Jones, J. R. Broach, Eds.(Cold Springs Harbor Laboratory, Cold Springs Harbor, NY, 1982)159-180.
35. H. Kondo, I. Miwa, J. Sunamoto, *J. Phys. Chem.* **86**, 4826(1982).
36. E. Bardez, et al., *J. Phys. Chem*,**88**, 1909(1984).
37. N. R. Clement, M. Gould, *Biochemistry*, **20**, 1534(1981).
38. K. Kano, J. H. Fendler, *Biochim. Biophys. Acta*, **509**, 289(1978).
39. D. Avnir, et al, *J. Non-Cryst. Sol.*, **99**, 379 (1988).
40. J. C. Pouxviel, B. Dunn, J. Zink, *J. Phys. Chem.***93**, 2134,(1989); B. Dunn, et al, in *Better Ceramics Through Chemistry III,* MRS Symp. Proc. Vol. **121**, 331(1988).
41. C. J. Brinker, et al, *J. Non-Cryst. Sol.*, 48, 47(1982); ibid, **63**, 45(1984).
42. Average pore diameter was estimated by the method of Kadokura [K. Kadokura, Ph.D. Dissertation, University of California, Los Angeles, 1983].
43. B. Quistorff, J. Dich, and N. Grunnet,"Preparation and Isolation of Rat Liver Hepatocytes", in *Animal Cell Culture*, J. W. Pollard and J. M. Walker, eds. (Humana Press, Clifton, NJ, 1989)151-160.
44. C. M. Peterson, L. Jovanovic-Peterson, and B. Formby, eds. *Fetal Islet Transplantation: Implications for Diabetes*, (Springer-Verlag, New York, 1988); C. M. Peterson, L. Jovanovic-Peterson, and B. Formby, eds. *The Second International Sansum Symposium on Human Fetal Islet Transplantation*, (Plenum, NY, 1995).
45. P. A. Tresco, *J. Controlled Release*, **28**,(1994) 253-258.
46. J. D. Andrade, J. Tobler, M. Lisonbee, and D. Min, in *Bioluminescence and Chemiluminescence*, A. A. Szalay, L. J. Kricka, and P. Stanley, eds. (John Wiley & Sons, NY, 1993) pp. 69-73.

Minimizing the Aggregation of Neutral Insulin Solutions

R. QUINN and J. D. ANDRADE ˣ

Received November 16, 1981, from the *Department of Bioengineering, University of Utah, Salt Lake City, UT 84112.* Accepted for publication October 21, 1982.

Abstract □ Various solution additives affect the solubility and macroaggregation of insulin in buffered aqueous solutions at physiological pH. The solubility of insulin may be improved with the addition of small amounts of aspartic acid, glutamic acid, EDTA (ethylenediaminetetraacetic acid), lysine, Tris buffer, or bicarbonate buffer. In addition, the propensity of dissolved insulin to reaggregate and precipitate may be inhibited by such additives. Buffered physiological (pH 7.4) saline solutions containing 0.001–0.003 *M* lysine in the presence of 0.005 *M* EDTA or 0.01 *M* lysine in the absence of EDTA improve insulin solubility and are effective in minimizing aggregation. Solutions thus prepared may be suitable for application in intravenous insulin infusion devices and may be useful commercial insulin preparations.

Keyphrases □ Insulin—minimizing aggregation, neutral solutions, lysine, solubility □ Aggregation—minimization, solubility of neutral insulin solutions, lysine solubility □ Lysine—minimizing aggregation of neutral insulin solutions, solubility □ Solubility—minimizing aggregation of neutral insulin solutions, lysine

The tendency of insulin solutions to form macroaggregates is an obstacle in the development of long-term insulin delivery systems (1–5). The macroaggregation of the insulin molecule often limits prolonged infusion to a few days unless the device is regularly flushed during the test period. This problem, as well as a desire to characterize the adsorption of insulin, have led us to search for a physiological solvent or additive that will stabilize insulin solutions. Insulin solubility and prolonged prevention of macroaggregation has been achieved by addition of various agents to dilute insulin solutions (4–8).

EXPERIMENTAL

The Tris buffer contained 0.1 *M* NaCl, 0.005 *M* EDTA (ethylenediaminetetraacetic acid) (Tris-HCl 14.04 g/liter; Tris, 1.34 g/liter)[1]. The phosphate-buffered saline solution was prepared using 1.36 g of Na_2HPO_4, 0.22 g of KH_2PO_4, 0.005 *M* EDTA, and 8.5 g of NaCl/liter (0.01 *M* phosphate and 0.145 *M* NaCl). The pH of both solutions was adjusted to 7.2–7.4, as needed, by addition of 0.1 *M* HCl or 0.1 *M* NaOH. Bicarbonate buffer was prepared using 1.428 g of $NaHCO_3$ and 8.070 g of NaCl diluted to 1 liter. A mixture of 5% CO_2 and compressed air was bubbled through the solution to adjust the pH to 7.4. Amino acids and other additives were added to the buffered solutions in varying concentrations as desired.

Crystalline insulin[2] at a potency of 25.2 U/mg was used in an attempt to regulate solution additives. Many other studies have used commercially available insulin preparations which usually contain additives that influence solubility and aggregation.

Solutions of 1 ml were sealed with paraffin film in 16-ml glass tubes (16 mm × 100 mm) and continuously agitated in a shaking water bath at 100–200 cycles/min and 37°. Solution turbidity was evaluated twice daily. The degree of aggregation of the solution was assessed visually on a five-plus scale: (+) meant clear, no observable particles, and (+++++) meant large aggregates or cloudy. Initially instrumental turbidity measurements were used to assess the degree of aggregation, but because of the macroscopic nature of the aggregate, this method did not accurately reflect the amount of aggregation. "First day" results indicate apparent solubility of insulin after 2–4 hr. The "5–6 day" results indicate degree of aggregation present at that time.

RESULTS

Additives tested were aspartic acid, EDTA, glutamic acid, bicarbonate buffer, ethanol, glycerol, leucine, lysine, and Tris buffer. When increased solubility or prolonged prevention of aggregation was observed, an attempt was made to determine the minimum amount of the additive required to produce the observed result. This was done by serially diluting the additive in the buffered solution while other buffer conditions were held constant. Results are given in Table I.

Ethanol, Glycerol, and Leucine—These three compounds proved to be very unsatisfactory as additives in the concentration range tested (0.001–0.1 *M*). None of the compositions demonstrated delayed onset

Table I—Effect of Additives on Insulin Aggregation

Major Additive	Buffer[a]	pH	EDTA (0.005 *M*)	Insulin Concentration, mg/ml	Effective in Blocking Aggregation?
Lysine (0.0005–0.1 *M*)	PBS	7.4	+	6–10	Yes
Lysine (0.0005–0.1 *M*)	PBS	7.4	–	6	Slight
Lysine (0.001–0.1 *M*)	PBS	9.0	+	6	Yes
Lysine (0.001–0.1 *M*)	PBS	9.0	–	6	Slight
Aspartic Acid (0.00005–0.05 *M*)	PBS	7.4	+	6	No
Aspartic Acid (0.00005–0.05 *M*)	PBS	7.4	–	6	No
Aspartic Acid (0.00005–0.05 *M*)	PBS	3.5	+	3–6	Yes
Aspartic Acid (0.00005–0.05 *M*)	PBS	3.5	–	3–6	Yes
Glutamic Acid (0.00005–0.05 *M*)	PBS	7.4	+	6	No
Glutamic Acid (0.00005–0.05 *M*)	PBS	7.4	–	6	No
Glutamic Acid (0.00005 0.05 *M*)	PBS	3.5	+	3–6	Yes
Glutamic Acid (0.00005–0.05 *M*)	PBS	3.5	–	3–6	Yes
Leucine (0.001–0.1 *M*)	PBS	7.4	+	6	No
Glycerol (0.001–1.0 *M*)	PBS	7.4	+	6	No
Ethanol (0.001–0.1 *M*)	PBS	7.4	+	6	No
Buffer A (0.005–0.1 *M*)[a]	PBS	7.4	+	6	Yes
Buffer A (0.005–0.1 *M*)	PBS	7.4	–	6	No
Buffer A (0.005–0.1 *M*)	Tris	7.4	+	6	Yes
Sodium Bicarbonate	$NaHCO_3$	7.2–7.4	+	0.5	Yes

[a] Key: (PBS) phosphate-buffered saline; (Tris) Tris buffer in 0.1 *M* NaCl.

[1] Chemicals were obtained from Sigma Chemical Co.
[2] Obtained from Calbiochem Behring Corp., La Jolla, Calif.; lot number 003622.

0022-3549/83/1200-1472$01.00/0

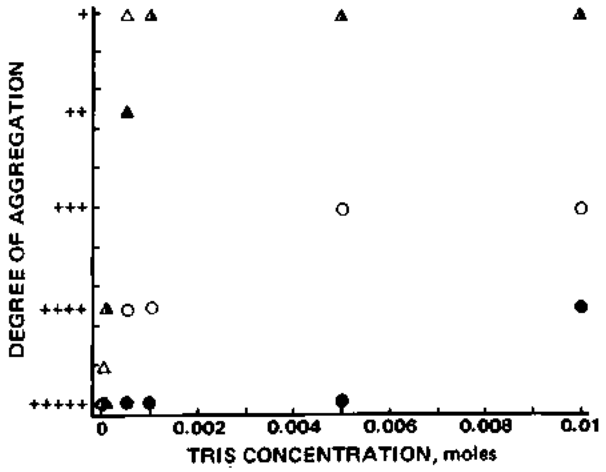

Figure 1—*Comparison of aggregation of insulin in phosphate-buffered saline as a function of Tris concentration. Solution conditions: phosphate-buffered saline, pH 7.2–7.4, temperature 37°, and insulin concentration, 6 mg/ml. Key: Degree of aggregation of solutions with 0.005 M EDTA at 1 (△) and 5 (▲) days; aggregation of solutions without EDTA at 1 (○) and 5 (●) days; (▲) point overlap.*

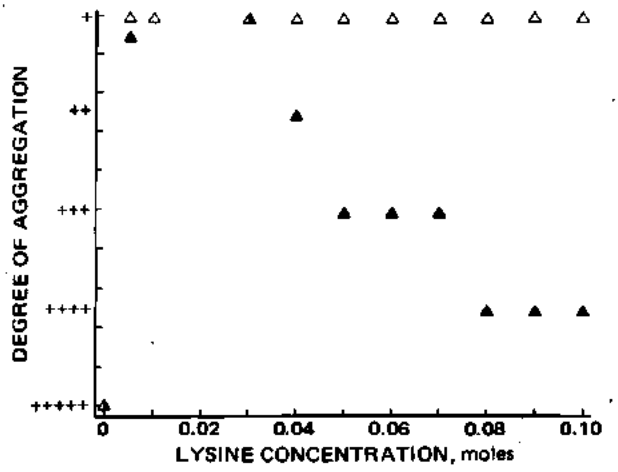

Figure 2—*Concentrations of 0.001–0.01 M lysine in 0.005 M EDTA and phosphate-buffered saline, pH 7.4. Key: degree of aggregation of solutions with 0.005 M EDTA at 1 (△) and 5 (▲) days; (▲) point overlap.*

of aggregation.

Tris Buffer—Phosphate-buffered saline solutions were prepared with and without 0.005 *M* EDTA, at various Tris concentrations (0.001–0.1 *M*). Figure 1 summarizes the aggregation of insulin as a function of Tris concentration in the presence and absence of EDTA, demonstrating that both additives are important in delaying the onset of insulin aggregation.

Lysine—Phosphate-buffered saline solutions containing lysine showed rapid dissolution of insulin, with the dissolution time decreasing as the pH was raised to 8.5–9.0. Solutions containing lysine at pH 7.2–7.4 maintained a clear, unaggregated appearance for 5–6 days. Higher lysine concentrations (0.1–0.01 *M* in 0.005 *M* EDTA) tended to aggregate more than those solutions containing lower lysine concentrations (0.01–0.001 *M*). Lysine (0.001 *M* in 0.005 *M* EDTA) is effective in minimizing aggregation (Fig. 2). However, when 0.005 *M* EDTA was eliminated from the phosphate-buffered saline solution, 0.01 *M* lysine was required to significantly minimize aggregation. Solutions of 0.01 *M* lysine and 0.005 *M* EDTA maintained at 4° without agitation remained not aggregated for periods up to 3 weeks.

Aspartic and Glutamic Acid—Earlier studies in other laboratories (5) showed that glutamic and aspartic acids were important in delaying the onset of aggregate formation. Our studies confirm the results of Bringer *et al.* (5) wherein aggregation was prevented for 6–7 days; however, serial dilution resulted in a decrease in the aggregation time. Aspartic acid proved to be more successful than glutamic acid at blocking insulin aggregation (Table I). It is important to note that due to the acidic nature of these amino acids, the pH of these solutions was 3.5 rather than 7.4. If the solutions were adjusted to pH 7.4, the aggregation was lost. This observation was also noted by Bringer *et al.* (5).

Bicarbonate—Two-milliliter solutions of sodium bicarbonate saturated with insulin were titrated to pH 6.3 with 0.1 *M* HCl, resulting in insulin precipitation. If solutions were back-titrated to pH 7.4 with 0.1 *M* NaOH the insulin remained undissolved. However, if a 5% CO_2–compressed air mixture was bubbled through the solution until pH 7.4 was reached, the insulin redissolved. A similar observation was noted by Lougheed *et al.*, where dissolution times were monitored as a function of bicarbonate concentration (8).

DISCUSSION

These results support the findings of previous researchers that agitation, additives, temperature, pH, and insulin concentration influence the solubility and macroaggregation of insulin. Recent work by Sato *et al.*, demonstrates that urea is effective in minimizing aggregation (9).

Several mechanisms for the prevention of aggregation have been proposed including the possibility of a serum substance (4) that prevents aggregation [newly published data from this group suggests that the bicarbonate concentration is the major factor in mediating insulin solubility (8)]. The chelation effect of the carboxyl groups of amino acids for zinc is believed to block aggregate formation by resulting in a more soluble form of insulin. This data is somewhat supported by the improvement of solubility and prolongation of aggregation time observed in solutions containing EDTA. As a chelating agent, EDTA may compete with insulin for zinc and, therefore, slow aggregate formation (10). Another possible mechanism for minimizing aggregation is that amino acid additives, especially lysine, may interact with the insulin molecule by hydrophobic and ionic means, thereby decreasing insulin–insulin interactions and preventing or slowing the formation of aggregates. More definitive work should be done with detailed analysis of the types of interactions and the conformation of the insulin molecule in these solutions.

Buffered physiological saline solutions containing 0.001 *M* lysine and 0.005 *M* EDTA improve insulin solubility and are effective in delaying the onset of macroaggregation. In the absence of EDTA, 0.01 *M* lysine solutions improve initial solubility and minimize the degree of aggregation. One advantage of the lysine additive is that the solutions are maintained at pH 7.4. A second advantage is that lysine is a common amino acid and is therefore not a synthetic additive.

Results summarized in this study emphasize the importance of additives in improving the solubility and stability of insulin solutions. It should be remembered that the type of insulin and additives used in various insulin preparations influence the properties discussed above, so a comparison of these results with other studies must be done with caution. The only way to accurately assess the contribution of each additive as to its solubility and aggregate-blocking properties is in a study such as this which minimizes the contributions of other solution variables or insulin additives.

REFERENCES

(1) B. Zinman, E. F. Stokes, A. M. Albisser, A. K. Hanna, H. L. Minuk, A. N. Stein, B. S. Leibel, and E. B. Marliss, *Metabolism*, **28**, 511 (1979).

(2) A. M. Albisser, B. S. Leibel, T. G. Ewart, Z. Davidovac, C. K. Botz, and W. Zingy, *Diabetes*, **23**, 389 (1974).

(3) W. D. Lougheed, H. Woulfe-Flanagan, J. R. Clement, and A. M. Albisser, *Diabetologia*, **19**, 1 (1980).

(4) A. M. Albisser, W. D. Lougheed, K. Perlman, and A. Bahoric, *Diabetes*, **29**, 241 (1980).

(5) J. Bringer, A. Heldt, and G. M. Grodsky, *Diabetes*, **30**, 83 (1981).

(6) H. Pekar and G. Frank, *Biochemistry*, **11**, 4013 (1972).

(7) P. D. Jeffrey and J. H. Coates, *Biochemistry*, **5**, 489 (1966).

(8) W. D. Lougheed, U. Fischer, K. Perlman, and A. M. Albisser, *Diabetologia*, **20**, 51 (1981).

(9) S. Sato, C. Ebert, and S. W. Kim, *J. Pharm. Sci.*, **72**, 228 (1983).

(10) T. Blundell, G. Dodson, D. Hodgkin, and D. Mercola, *Adv. Protein Chem.*, **26**, 279 (1972).

ACKNOWLEDGMENTS

Funded by the Kroc Foundation. We thank G. Iwamoto for helpful suggestions in this work.